Carbon Nanocones as Anode Material in Lithium Ion Batteries

Marius Uv Nagell

December 15, 2010

Acknowledgments

I would like to thank my supervisor Associate Professor Fride Vullum-Bruer for her help and guidance, my co-supervisor Morten Andreas Onsrud for his guidance and support in the laboratory as well as SEM images and XRD results, Edel Sheridan, Ann Mari Svensson, Carl Erik Lie Foss, and Phung Tran Hieu Dinh for help during the experiments and writing, and Conor P. McCarthy for SEM imaging and laboratory support.

A thank also to Celgard for their free separator samples, and n-TEC for their carbon nanocones.

And finally a thank to Audun Nystad Bugge and Molly Strimbeck Bazilchuk for providing a computer screen during the final writing period, making it possible to finish writing this report.

Abstract

A carbon material containing carbon nanocones was used as an anode material in lithium ion batteries. The carbon material was tape casted onto copper before being assembled into batteries with lithium metal as the cathode. The anode showed good results compared to other materials, with emphasis on the initial charge capacity. There were a spread in this capacity, but they were all between 480 and 780 mAh/g. However, initial results also showed a very large irreversible capacity loss between 220 and 360 mAh/g.

Contents

Chapter 1

Introduction

Lithium ion batteries are used in a wide variety of products, especially light, portable applications, such as mobile phones, portable computers and cameras. Figure 1.1 shows a comparison of different battery technologies, where lithium ion batteries have one of the greater potentials. Lithium metal was first used in the 1970s as an anode material in batteries. These batteries showed high energy densities and high capacity, compared to the commercial batteries at that time. However, there are concerns for this battery technology. Lithium is a highly reactive metal and this leads to safety problems. Incidents with commercial batteries have occurred as the batteries were not safe enough. In some cases the cases the batteries created so much heat that they exploded. As the lithium ion batteries are rechargeable, another occurring challenge is the number of charging and discharging cycles they can withstand before they become exhausted. This problem has to do with the volume changes in the electrode materials as the process mechanisms involve intercalation and deintercalation of charged species [1].

If you compare the first commercially available batteries with the batteries of today, there are no major differences [2]. They still employ the same principles. However, extensive research have produced better electrodes, safer electrolytes, leading to improved capacity and cycling life time.

Many research groups have focused on carbon anodes to see how much they can exceed the stoichiometric limit of lithium ion intercalation of graphitic carbon, LiC_6. This will yield a theoretical capacity of 372 mAh/g [2]. Carbon anodes are used in many commercial lithium ion batteries today. Everything from amorphous carbon and kish carbon to carbon nanotubes have been explored in different varieties and with different results. There is a trend of evolving the carbon anodes, but the limitations of the material could soon be reached. As a result, several other materials have also been investigated, although none have become commercialized like carbon. One of few carbon materials that have yet to be tested is carbon cones. This material consists of conic layers of graphene which could imply that they have similar properties as other graphene anodes.

Carbon cones were first observed in 1994 [3]. In Kværner's carbon black and hydrogen process [4] they managed to create a substantial amount of this material in which were accidentally discovered in 1997 [5]. This following project investigates carbon cones as potential anode material for use in lithium ion batteries. The processes of producing anodes by tape casting slurries

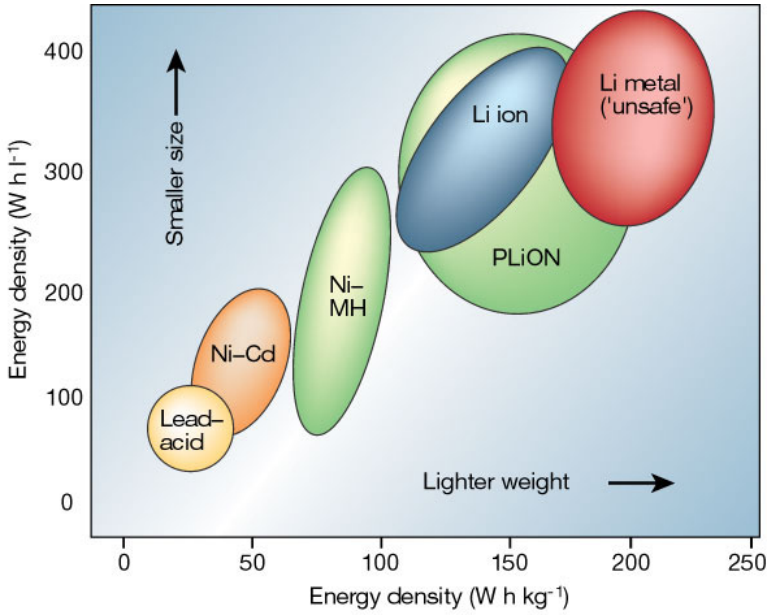

Figure 1.1: Comparison of battery technologies with emphasis on energy density [6].

containing carbon nanocones is described. These anodes were used in small button cell batteries which were characterized by charge/discharge measurements.

Chapter 2

Theory

2.1 Lithium ion batteries

2.1.1 Lithium ion battery principles and requirements

The basic principle of lithium ion batteries is that lithium ions go back and forth between electrodes, as shown in figure 2.1, through an electrolyte. This is also the reason for its alternative name, rocking chair batteries [2]. When a battery is charged the ions move from the cathode to the anode, and when it is discharged the opposite occurs. Intercalation is the process where a small ion is inserted into the electrode material, and becomes a stable part of a structure. Deintercalation is the reversed process. These processes are accompanied by a reduction or oxidation reaction which should be highly reversible to sustain good cycle ability for a great amount of charge/discharge cycles [7, 8]. These processes will induce a volume change as ions go in and out of the original structure. Volume changes will over time deteriorate the electrode structures. Reducing these small volume changes are therefore an important target for developing electrode materials. The most common strategies used to reduce the volume changes are development of different alloys, doped, or undoped ceramic materials, or nanostructures.

Lithium ion batteries are being used in different consumer products, ranging from mobile phones and portable computers to power tools and electric vehicles. This means that different batteries need different properties, but mainly the need for high amounts of cycles as well as a good capacity are the most important requirements. The number of cycles depends on the anode and cathode materials fatigue rate. As the intercalation and deintercalation processes continue, the materials experience a continuous volume change. Unfortunately, not all of the lithium ions intercalate and deintercalate. They can also take part in side reactions on the electrodes. This will mean that the number of lithium ions available for further cycling is decreased.

Battery capacity is defined as the electrical energy content or the amount of current a battery has delivered when completely discharged after one hour (Ah) [9]. In the literature gravimetric capacity is a more common capacity measurement. Gravimetric capacity is the mass specific capacity and is given in ampere hours per gram (Ah/g) [10]. Another measured capacity is volumetric capacity. This is the volume specific capacity, ampere hours per liters (Ah/l). Higher mass specific capacity gives lighter batteries and higher volumetric capacity gives possibilities

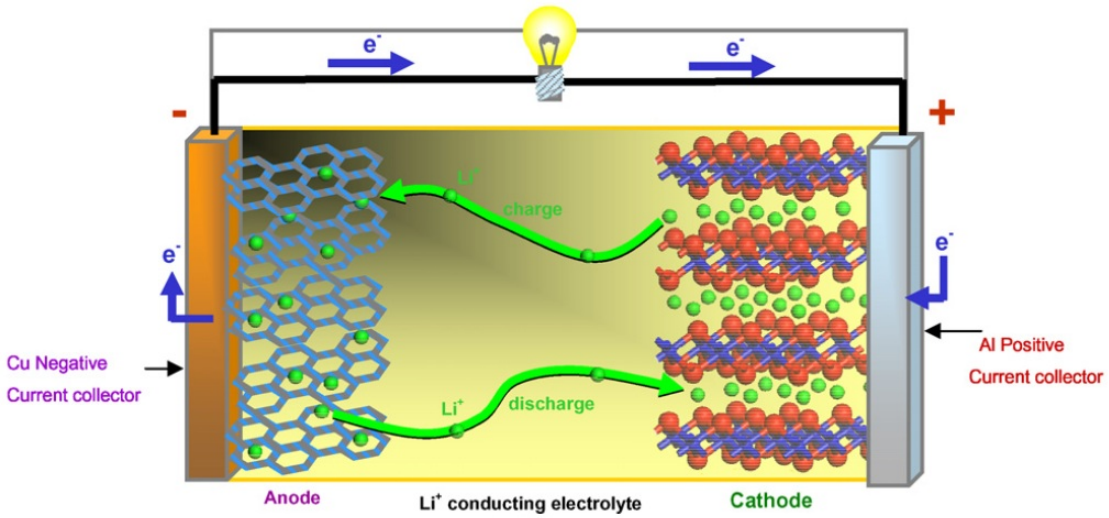

Figure 2.1: An overview of the intercalation process in a lithium ion battery.

of smaller batteries, see figure 1.1. Looking at the energy content is also useful. This is given in either specific energy (gravimetric energy density) or energy density (volumetric density). They are measured in watt hours per kilogram (Wh/kg) and liters (Wh/l), respectively. To get high gravimetric and volumetric energy density it is important to have high gravimetric capacity as well as high charge density. This means that there has to be a high number of charge carriers per mass and volume unit [8]. These are criteria which separate a good battery material from a less good one. Measuring this can be done by applying charge/discharge cycles on the batteries.

For each charge and discharge there will be a charge capacity and discharge capacity measured. The difference in charge capacity and discharge capacity is called irreversible capacity [11]. This is an indicator of how much of the lithium irreversible processes like the formation of solid electrolyte interfaces and other side reactions. The Columbic efficiency, also known as faraday efficiency, is the ratio between the discharge and charge capacity [12]. It is a good indicator of loss in capacity, hence a good battery has to have a good Columbic efficiency for every charge/discharge.

The number of cycles the battery handle is also possible to measure. It is more commonly called lifetime. Testing the lifetime takes a long time as a good lifetime would consist of a great number of cycles. Lifetime is also dependent on the duration of one cycle. Having a mobile telephone battery witch uses 5 days on a cycle and has a lifetime of 1000 cycles, would be nice, but is not necessary because the mobile phone would probably not withstand 13 years of use. This indicates that the lifetime of a battery is of different importance for different applications. Some applications would benefit from long cycle times and some from high amount of cycles.

Batteries with $LiCoO_2$, $LiNiO_2$, and $LiMn_2O_4$ cathodes and carbon anodes have shown a lifetime of 300 cycles, and potentials of about 4 V [13]. This is good for consumer electronics, but for electric vehicles, batteries with longer lifetimes are needed. Lifetimes of over 8000 cycles has been proposed as requirement. A $LiFePO_4$ cathode and anatase TiO_2/graphene com-

posite anode gave a 1.48 V discharge voltage battery which lasted for over 700 cycles with a Columbic efficiency of around 100% the whole time [14]. Hence, showing potential for far more cycles. Another promising result has been given by $LiFePO_4/Li_4Ti_5O_{12}$ combination cell, which is claimed to manage 15 years of use [13]. This would be equivalent to over 10000 cycles if charged twice a day. These two materials are considered having large potential for making long lasting batteries, especially for electric vehicles. $LiFePO_4$ has already been chosen by light electric vehicle users in areas where low temperature performance is not required [15].

2.1.2 Anodes

The anode is the electrode that receives the lithium ions upon charging. These materials have to be able to intercalate a great amount of lithium ions into their structure and deintercalate efficiently upon discharge. On the battery market today, most lithium ion batteries have anodes consisting of different types of carbons. Researchers are constantly trying to enhance the anodes using new forms of carbon by making different structures, alloying carbon with other materials, and trying out new materials. Another material of special interest is silicon. Both of these are being further described here.

Carbon

Carbon is the most commonly used anode material. The stoichiometric limit of intercalated lithium ions in graphitic carbon is six carbon atoms per lithium ion, LiC_6. This yields a theoretical capacity of 372 mAh/g [2], but could be overcome by changing the stoichiometry.

Carbon based anodes is preferred because compared to many other alternatives, carbon experiences little volume change upon intercalation and deintercalation. Graphite only increases with 9.4% in volume when lithiated to LiC_6 [2]. Perfect graphitic structures can reach the theoretical limit, but amorphous carbons are thought to have higher potential lithium uptakes than the stoichiometric limitation of LiC_6 [16]. Altering the micro and nano structures of carbon particles can also increase the capacity. Artificial graphite was developed by optimizing particle and pore size in the material [17]. Anodes made by this material showed a specific capacity of 360 mAh/g with 95% columbic efficiency, and it could sustain high discharge rates.

Modified natural carbon and artificial carbon exhibit great potential for reaching specific capacities above the theoretical maximum. Air oxidation of natural graphites has improved the electrochemical characteristics and kish carbon show intercalation capacities above 372 mAh/g [18]. Many other varieties of carbon have been tried too, like carbon nanotubes (CNTs).

Tin filled CNTs has been investigated as anode material, and showed promising results with specific capacities above 700 mAh/g for 40 cycles [19]. The problem with this material is the high irreversible capacity and the high cost which make them less attractive for commercial use. Another way of using CNTs is to align them on a substrate. This does not remove the high irreversible capacity which the CNT has, but one test showed a stable discharge capacity of 265 mAh/g over 50 cycles [20].

Silicon

An opponent to the carbon based anodes is silicon. Silicon has a theoretical capacity of around 4200 mAh/g [2, 7], which greatly exceeds the values of carbon. This corresponds to a stoichiometry of Si_5Li_{22}. The problem of this material is the volume change it experiences during intercalation and deintercalation. The volume change is observed to be between 300-400% [2, 7]. As an alternative to replace carbon as anode material, silicon research needs to focus on eliminating its expansion problem, but without losing too much of its potential capacity. This is the primary problem of silicon anodes and has been the biggest hindrance for commercialization.

Solutions to the volume expansion would be to give room to the expanding volume by creating different nanostructures. Quantum dots have been used as an alternative. Coated with amorphous carbon these particles were used and resulted in a first charge capacity of 1257 mAh/g [21].

One research group tested the potential of a silica-carbon composite [22]. This gave a reversible capacity of around 710 mAh/g for 100 cycles, which is a very good result. In an attempt to overcome the silicon's volume expansion a group made silicon nanowires [23]. For 20 cycles the capacity of the batteries were around 3500 mAh/g which is an exceptionally high capacity.

2.1.3 Cathodes

The cathodes are materials which should deintercalate lithium ions upon charging. This gives a high demand to structure stability of the material, as well as low energy barrier for deintercalation. There are three common types of anodes used in lithium ion batteries; layered lithium-metal oxides, lithium-manganese spinels, and polyanionic compounds, usually called olivines.

The most common metals for layered lithium-metal oxide ($LiMO_2$, M = Ni, Co, etc.) cathodes, figure 2.2a, are nickel and cobalt. Both lithiated nickel and cobalt oxide have high structural stability in the 3 to 4.1 V range [2]. The layered structure can be seen in figure 2.2a. Extensive use of cobalt and nickel has its drawbacks and the main problem is that there are limited resources.

The spinel structure Mn_2O_4, shown in figure 2.2b, is an ideal framework for lithium ions as it allows both intercalation and deintercalation of lithium [24]. Lithium-manganese spinel ($LiMn_2O_4$) cathodes can offer advantages such as high thermal threshold, excellent rate capability, minimal health and environmental issues, and low price [2]. It is thought to replace $LiCoO_2$ cathodes in commercial batteries, but it needs some improvements.

The most stable and usable olivine structure is the $LiFePO_4$, shown in figure 2.2c. $LiFePO_4$ is non-toxic, has low capacity fade, a flat discharge plateau, low volume expansion, and a capacity of $150-170$ mAh/g [8, 25]. The problems with this material are the poor conductivity [8, 26] and its sensitivity to impurities, especially Fe^{3+}.

2.1.4 Electrolytes

Electrolytes is a medium containing lithium ions and which allows for transport of these ions between the electrodes. It is therefore an essential component for the battery to work properly. There are many approaches to making an electrolyte and the standard method is to solve

(a) Layered lithiated metal oxide (b) Spinel, $LiMn_2O_4$ (c) Olivine, $LiFePO_4$

Figure 2.2: The three main cathode structures [2].

a lithium based salt in a solvent. The solvents can vary from simple liquid solvents, to solvents held in place in porous membranes, or even polymers. Polymer electrolytes are not as common as solution based electrolytes. They are more attractive, though, because they are non-flammable [2, 27].

One of the most common electrolytes is $LiPF_6$ in ethylene carbonate (EC) and dimethyl or diethyl carbonate (DMC and DEC, respectively). This is, as a lot of other electrolytes, a compromise between advantages and disadvantages. It is flammable and only electrochemically stable up to 4.5 V [2], but it is not explosive such as $LiClO_4$ or as poisonous as $LiAsF_6$. $LiPF_6$ can also be decomposed to HF, which can be a problem if the batteries overheat and explode or leak [28]. Implementation of manganese based cathodes, as earlier mentioned, would demand removal of $LiPF_6$-based electrolytes. The reason for this is that they do not work very well together, because of the HF created. This is an example of the fact the use of electrolyte should be adapted to the electrodes used.

2.1.5 Solid electrolyte interfaces

During the first charge/discharge cycle of the lithium ion battery, there will be some decomposition of the electrolyte into inorganic species like Li_2CO_3, Li_2O, LiCl and organic polymeric species like R-OCO_2Li (R is a hydrocarbon chain) [29]. These components together with other species depending on the system, will deposit on the electrode surface to produce a solid electrolyte interface (SEI) [29, 30]. This happens on carbon anodes as well as other electrode material. The irreversible capacity of electrode materials is partially caused by the SEI formation.

The SEI is not only a problem. This layer protects the electrodes from other decomposition reactions that can occur. Controlling the SEI formation is important. Too thick SEI will create a high resistance film and lithium ions will not be able to easily intercalate in the carbon anode. To control the SEI the surface reactions and properties need to be characterized. This project will not investigate this, but still keep in mind the occurrence of the SEI and its effects on the anode.

2.2 Carbon nanocones as anode materials

2.2.1 Carbon materials

Carbon comes in different structures, such as diamond, graphite, fullerenes, graphene, carbon nanotubes, and carbon nanocones [1]. The latter is the least known and comes from Kværner's carbon black and hydrogen process [4]. Carbon nanocones is the material investigated in this project.

Diamond is formed under high pressure and temperatures. The diamond is a very hard and stable material and is used in everything from jewelry to drill bits. Graphite on the other hand, is used in pencils and as electrodes for different electrochemical applications. This is also a crystalline material, but does not exhibit the same properties as diamond. It is highly conductive, whereas diamond is an insulator, and it is more brittle.

Carbon nanotubes [31] and fullerenes [32] are two other materials, found much later (1991 and 1985, respectively) than diamond and graphite. The carbon nanotubes (CNTs) are small tubes which have proven to be far stronger that steel [33] and can be either semiconducting or conducting [34]. They can have single or multiple walls and have a lot of possible applications, ranging from capacitors to reinforcement in composites. Fullerenes on the other hand, are a family of ball shaped molecules consisting of carbon pentagons and hexagons. The smallest stable, and most common, fullerene is the C_{60}, but structures as C_{70}, C_{84} and C_{100} are found too. They are thought to be used as everything from containers for small ions to superconducting materials in structures with alkali metals (A_3C_{60}, A - alkali metal) [35].

Graphene is only single sheets of hexagonally honeycomb structured carbon, while graphite is blocks of layered graphene. Graphene was first isolated and characterized in 2004 [36], and has been shown to be a versatile, strong, conductive, and transparent film. This gives raise to different uses like a transparent conductor [37].

Carbon nanocones, which are the focus of the current work, were first observed by Klaus Sattler and Maohui Ge from the University of Hawaii in 1994 [3]. They observed nanocones of sizes up to 24 *nm* in length and 8 *nm* in diameter of the cone opening. They made the nanocones with vapor condensation of carbon on a graphite substrate and later did scanning tunneling microscopy (STM) studies of their product. Applications have not been reported, but several research groups have investigated basic properties of the carbon nanocones.

Carbon nanocones

The carbon material from Kværner's Carbon Black and Hydrogen Process [38] is a material which consists of cones, disks, and impurities of carbon black. The discs make up around 70% [39] of the powder, whereas the angled nanocones make up only about 20% [39] of the powder. The rest is impurities of carbon black [39]. Carbon nanocones have five different angles, depending on how many defects there are in the apex of the cone. The mentioned defects are missing carbon atoms in the apex, as shown in figure 2.3, which creates one or more pentagons in the graphene sheet and forces the sheet to bend into a cone. The more defects the smaller angle of the cone, which is given by the following relation:

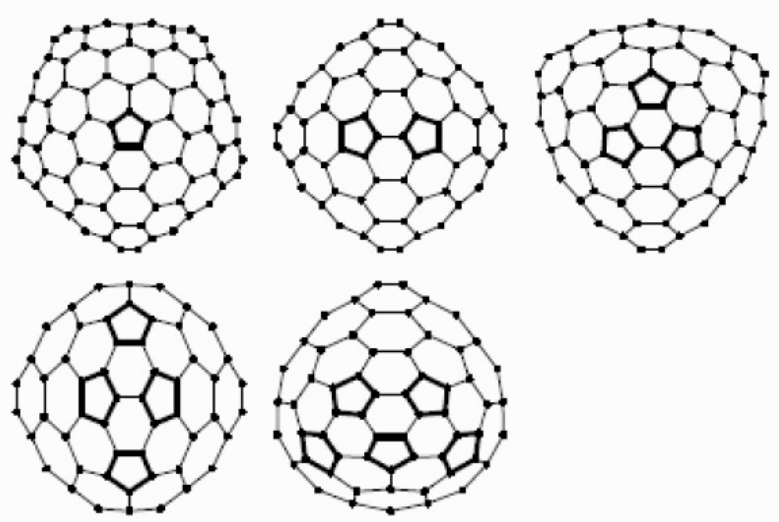

Figure 2.3: The five defects that make carbon cones [38].

$$\sin(\frac{\phi}{2}) = \frac{2\pi - p \cdot \frac{\pi}{3}}{2\pi} \tag{2.1}$$

Where ϕ is the possible angles and p is the number of defects ranging from 0 (flat discs) to 5 which gives an angle of 19.2° [40]. This restriction in number of cone angles rises from the geometry and limitations of the honeycomb structure of the sheets that bend. If more defects are introduced it would simply not be an open cone. The nanocones are not only single cones, but layers of cones with wall thickness of 20 *nm* to 50 *nm* and opening diameters roughly between 0.8 μm up to 3 μm [38]. The outside layer of the cones consist of amorphous carbon. SEM images of carbon nanocones can be seen in figure 2.4.

Application of the carbon nanocones as anode material has not previously been reported. As it consists of both amorphous and crystalline carbon it should be highly possible for the cones and disks to be used in lithium ion batteries. Carbon nanocones have been investigated as a potential thermal rectifier material by Yang *et al.* [41].

2.2.2 Recent development

There are numerous reports on different anode materials, especially carbon anode materials. None of them mention carbon nanocones, but their results give indications of where good results should lie. Yoo *et al.* tried out different versions of a type of modified graphene. This was graphene nanosheets combined with carbon nanotubes or fullerenes [42]. The carbon nanotubes and fullerene combinations, as well as the pure form of graphene nanosheets, all had gravimetric capacities above the theoretical value. 730, 784, and 540 mAh/g, respectively. After 20 cycles the values decreased to 480, 600, and 290 mAh/g, respectively. Wu *et al.* [43] investigated the capacity of hard carbon, which is said to not have more than about 250 mAh/g capacity. Their result for hard carbon was a capacity of 252 mAh/g, but they had also doped hard carbon

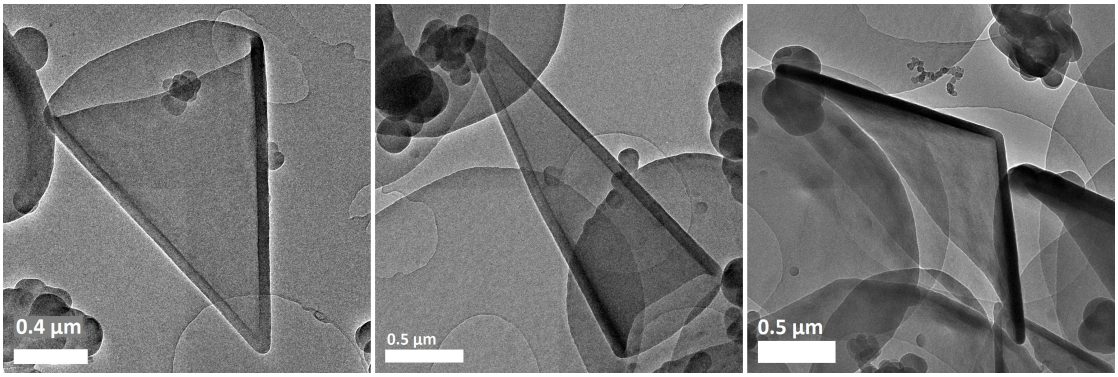

Figure 2.4: Three different sized cones with 1 (right), 4 (left), and 5 (middle) defects. [Images: Morten Onsrud].

with boron oxide, B_2O_3, and found out that 15.3 wt% was the optimal amount which gave a capacity of 394 mAh/g. This is barely above the theoretical value for carbon, 372 mAh/g, and several other reports have exceeded this value. Su *et al.* did not exceed the theoretical capacity with their hollow carbon shells [44]. They tried to dope their carbon shells with nitrogen as well, but achieved the same results, 325 mAh/g, after both 1 cycle and 100 cycles. This shows good stability of the material. Su *et al.* concluded that the higher the crystallinity of the carbon anode, the higher the electrical conductivity, and therefore it could be thought that higher crystallinity would give better cycle ability at higher currents. Y. Wang *et al.* tried to make carbon anodes of carbon nanospheres of diameters less than 100 nm with nitrogen-functional groups prepared by carbonizing polypyrrole nanospheres [45]. These spheres showed an initial capacity of 420 mAh/g and after 60 cycles showed a capacity loss of 0.15% per cycle. Q. Wang *et al.* used hard carbon spheres with mesopores. The spherule size was in the range of 6.5 μm. These spheres gave a reversible capacity of 430 mAh/g, and by modifying the spheres surface by dispersing it with 100 nm particles of SnSb the capacity was increased to 480 mAh/g. Khomenko *et al.* [46] investigated a variety of different carbon and carbon/silicon composite materials, which gave the results in figure 2.5.

2.2.3 Slurry processing

Producing carbon nanocone anodes is not does not consist of just adding the carbon nanocone powder to a current collector and assemble this into a battery. The powder needs to be mixed into a slurry which can be controlled and further be casted on the current collector material. The current collector is a thin copper film.

Mixing the slurry properly is important. Consistent slurry mixing will make sure that the casted film thickness is controllable. It is important to know the viscosity of the slurry as this will give answers of how the slurry behaves at different shear rates, which can be applied to the casting processes.

The thickness is important as it can alter the internal pressure of the battery, which will affect the results. Another reason to control the thickness is the amount of active material used. If the

Materials	Content of Si (%)	Reversible capacity ($mAh\,g^{-1}$)	Irreversible capacity ($mAh\,g^{-1}$)
PUREBLACK®	–	160	215
PUREBLACK®	20	625	225
Hard carbon	–	195	155
Hard carbon	20	620	380
Graphite	–	358	26
Graphite	5	475	45
Graphite	10	590	70
Graphite	15	706	125
Graphite	20	830	170
Graphite	40	1235	440

Figure 2.5: A table from Khomenko *et al.* which shows the capacity and irreversible capacity of different carbon materials [46].

anode film is too thick, the material near the current collector will not be used. Too thin anode film and the maximum potential for the anode is not being used. This makes it important to control the thickness to be sure that the right amount of active material is used, as well as having a reproducible film. The main focus in this project is to find a good process for making anodes by creating reproducible casts of desired thicknesses.

2.2.4 Additives

Binder

The anode usually consists of carbon. Carbon itself will not automatically stick to the current collector. Therefore a binder material is needed to keep a good contact between the carbon and the metal current collector. The binder also gives the electrodes enhanced mechanical strength. An ordinary anode is composed of 90-95 wt% carbon which is held together by 5-10 wt% of a polymeric binder.

A problem with the binder material, is that it has a negative effect on the electrochemical characteristics of the anode and cathode [47]. Choosing an appropriate binder is therefore important. Polyvinylidene fluoride (PVDF) is a commonly used binder for carbon materials. The reason for using this polymer is that it provides chemical stability, reversibility, chemical resistance, and good wettability, as well as being inexpensive [48].

2.2.5 Safety issues

Preventing thermal runaway or chemical breakdown during use of the battery should be an important target in battery research. Lithium is a reactive metal and reacts violently in an oxygen atmosphere or when exposed to water [28]. Usually the failure of the lithium ion batteries are caused by short circuits inside the battery, as well as exposure to high temperatures or overheating during charging and discharging [49, 50]. Leakage of electrolyte and exposure to water are also sources to dangerous failure mechanisms. Reasons for internal short circuiting could be deposition of lithium dendrites on the carbon anode which penetrate the separator [49]. Another

reason could be contaminations of metals in the electrolyte which could start other unwanted reactions or just short circuiting of the system [50].

Electrolytes

The electrolyte solvents used in lithium ion batteries today have low boiling points and flash points around 30°C. Replacing these with low- or non-flammable electrolytes is an important step towards safer lithium ion batteries. This would prevent the risk of explosion and thermal runaway [2].

The batteries today use electrolytes which have a tradeoff between cell performance and flammability. The flammability can be reduced by using additives, but in most cases it will affect some of the performance as well. Fluorinated and organo-phosphorus compounds are amongst the most investigated additives [2, 51]. The flame-retardant trimethyl phosphate has been studied as an additive as it is chemically stable on both the cathode and the anode side in lithium ion batteries [51].

Separators

In a battery the electrode must never get in contact with each other. If they do, the battery will short circuit and become destroyed. To prevent this from happening, separators are used. These are porous films which allow for ions and electrolyte to flow around on each side, but at the same time prevent contact between the electrodes. Separators have to be thin films so they do not take up any extra space in the battery. Neither can they react with the electrolyte, anode, or cathode. Porous polymer films are often used as separators, as they are usually inert and easy to produce [52].

2.3 Rheology

To better understand a slurry, more that the properties visible to the naked eye needs to be characterized. Knowing the rheology, in this project mainly the viscosity, gives knowledge of how the slurry behaves. This can be related to the casting process and from there give answers to how the thickness of the casted films best can be controlled. To understand this, some fundamental knowledge of how viscosity work is essential.

2.3.1 Viscosity theory

Noncrystalline materials which are exposed to stress and deformations have, as solid materials, a certain resistance to the deformation force. Where crystalline materials deform by dislocations, these noncrystalline materials deform by viscous flow [54]. These materials are called fluid materials [55].

Fluid materials can be everything from liquid or polymer solutions to hard particles in solvents. The property of viscous flow is called viscosity and can be determined on a macroscopic

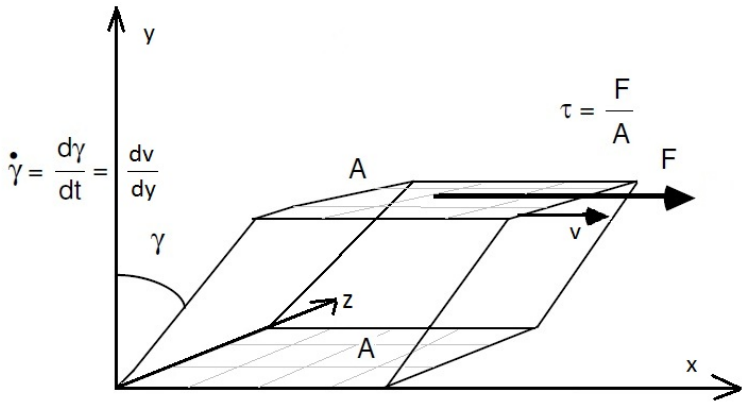

Figure 2.6: A liquid moving at share rate $\dot{\gamma}$ under an applied stress τ [53].

scale. By looking at two parallel plates, shown in figure 2.6, the viscosity is given by the following formula:

$$\eta = \frac{F/A}{dv/dy} \tag{2.2}$$

Where F is the applied force, A is the area of the plate, dv is the change in velocity perpendicular to the distance normal on the two parallel plates, and dy is the change in distance between the parallel plates [54]. This can be rewritten into shear stress, τ, and shear rate, $\dot{\gamma}$ [53]:

$$\eta = \frac{\tau}{\dot{\gamma}} \tag{2.3}$$

Viscous systems can be divided into two main fluids; Newtonian and non-Newtonian. Newtonian fluids have viscosities which are independent of the shear rate. This gives a constant viscosity for any shear rate and a linear relation between the shear stress and shear rate. A non-Newtonian fluid has a shear rate dependent viscosity leading to a non-linear relation between the shear stress and shear rate. Both are shown in figure 2.7.

Dilute particle solutions

Particles in a solution will come in contact with each other, especially before becoming homogeneously dispersed. The contact will create friction, which is a contribution to the viscosity of the solution. A solution with single isolated particles was found by Einstein to have the following viscosity relation [56]:

$$\eta = \eta_0(1+2.5\phi) \tag{2.4}$$

Where η_0 is the solvent viscosity and ϕ is the volume fraction of the spheres in the solution. The more solvent there is, the lower the viscosity will be. But this does not take into account particle size distribution or particle geometry. Taking in account the geometry, the viscosity quickly becomes very complex.

Smaller particles can enter voids between larger particles, creating more particle friction which will increase the viscosity. Smaller particles will also give higher viscosity [57] due to the increased surface area, which again gives room for more friction.

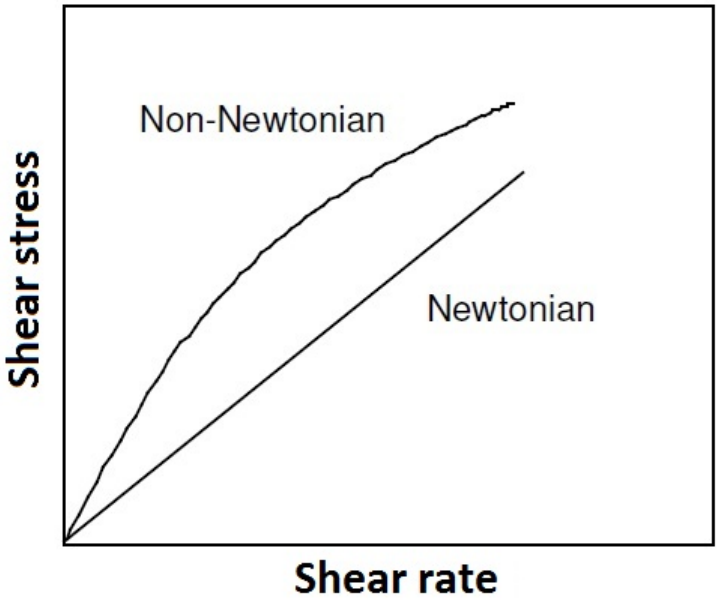

Figure 2.7: Plot of shear force vs. shear rate for a Newtonian and a non-Newtonian fluid [53].

Polymer solutions

Polymers are not hard particles. This makes the viscosity somewhat different to calculate than for solid particles. Molecular weight, polymer-polymer, and solvent-polymer interactions are the three most important factors for polymer solutions. The interactions would decide the size and form of the polymer particle. Size and form are important factors in the solid particle solutions, and would be important for polymer solutions too. Polymer-polymer interactions would decide how complex and strong the polymer network would be. This will, under shear stress, be deformed and possibly destroyed, which would alter the viscosity to some degree. The ability to recreate this network would make a difference in viscosity over time. If the networks are getting more complex, the viscosity increases [55]. Molecular weight is an indicator on the size of the molecules. Higher molecular weight gives larger polymer molecules. Larger polymer molecules give more possibilities to make networks, and could contribute to higher viscosity [57].

Complex fluids

In many cases fluids do not only consist of a simple system of components, and the dividing into Newtonian and non-Newtonian fluids becomes inadequate. Actually, as good as every complex fluid system is non-Newtonian, so a more thorough classification of behavior is needed.

Liquids can behave differently at different shear rates. Some become less viscous as the shear rate increases, and they are referred to as shear thinning fluids. Others are known to become more viscous at higher shear rates and are called shear thickening fluids [55]. Shear

thickening, or dilatancy as it is called, is the phenomena that happens in quick-sand. Quick movements and hasty panic attacks makes the sand viscous and impossible to escape from, but calm, slow movements will get you out.

Fluids can have a critical stress point, where applied stress below this critical stress will not affect the fluid. The stress above this critical point, the yield stress, will make the fluid flow. Fluids like ketchup behave like this, and they are called Bingham fluids [55]. Some fluids do not behave as Newtonian fluids after the yield stress is reached. They show a plastic flow, which means they become shear thinning. Toothpaste and lipstick are two examples of this [55].

Pseudoplastic fluids are fluids which do neither have a critical stress point nor a Newtonian behavior. They will flow instantly upon applied stress and in most cases show shear thinning tendencies. Fluids that can have this behavior are paint, bread dough, and polymer solutions [55].

For most fluids, the viscosity is independent of time, but for some the situation is different. Many concentrated dispersions need time to reach a steady viscosity upon applied stress, or shear rate. Stabilization is dependent on the internal stabilization of network structures that might have been broken by the shear stress. This will require some time to rebuild. Equilibrium between breakdown and rebuilding of the structure creates a time dependent steady state which will determine the viscosity at the shear rate. Thixotropy is the name of this phenomenon. When the shear rate is reduced, the stress graph will form a hysteresis loop which ends up lower than the starting point. The area of this hysteresis loop, such as that of figure 2.8 then represents the energy used to do the structure breakdown [55].

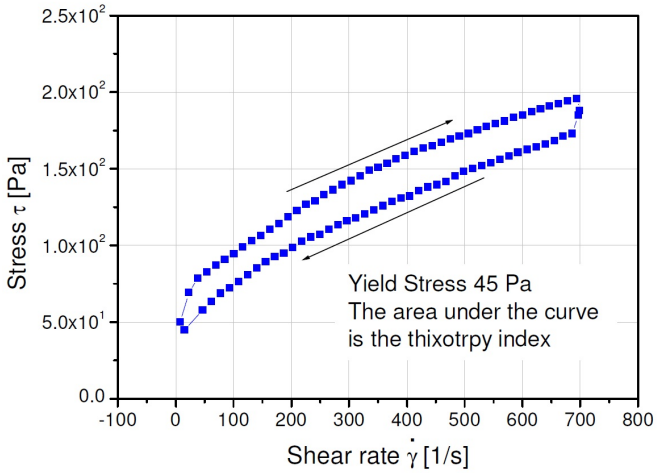

Figure 2.8: A hysteresis loop of a thixotropic material [55].

Whereas a thixotropic fluid gets a decrease in viscosity over time at a constant shear, a fluid which viscosity increases is called a rheopectic fluid. The viscosity-shear rate curve for these fluids will make a repeatable hysteresis loop. There are fluids which behave similarly, but do not have this hysteresis loop that can be repeated indefinitely. This would separate a real rheopectic fluid from a non-real one [55].

2.3.2 Carbon and PVDF

Most of the anode material used today consists of carbon and a binder. The most used combination is carbon and PVDF. PVDF will cover an amount of the carbon particles surface and create a complex network of particles. The size and geometry of the particles will decide the amount of reactive sites for the polymer. PVDF creates hydrogen bonds with the carbon particles [57]. These bonds help create a viscous slurry which again will create a mechanically strong casted film.

Experiments on slurries made of carbon, PVDF and NMP showed shear thinning behavior of the slurry. This was created by the fact that the networks of polymer and particles could not withstand the gradually increasing shear rate [57]. For casting purposes this is desirable as the high shear when casting would make it easier to cast the film. The tape casting process gives high shear rate, which makes it easy to spread the slurry evenly. After the casting, the shear rate decreases and the film stays viscous and does not start to flow.

Other factors that affect the viscosity of this slurry are the surface area of the carbon and molecular weight of the polymers [57]. Higher surface area of the carbon particles gives higher viscosity of the slurry. This relates to the number of reactive sites on the carbon particles. More active sites imply more places for the polymer to create hydrogen bonds. Higher molecular weight also increases the viscosity. Larger polymers can bind to more carbon particles and make more viscous slurries.

A more homogenous PVDF distribution in a carbon slurry gives a more viscous slurry [57]. This would make it possible to determine whether the system is properly mixed by measuring the viscosity of the slurry. Using this in similar systems can give indications on distribution of the PVDF. A homogenous dispersion is important as aggregated areas of PVDF would lead to reduced conductivity and hinder intercalation of lithium in those areas.

Chapter 3

Experimental

3.1 Equipment

- Ball mill - RETSCH PM 100, planetary mill
- Glove Box - MBRAUN LABmaster SP
- SEM - Zeiss SUPRA 55 VP FESEM and Hitachi S-3400N
- Rheometer - Physica MCR 300
- Tape caster - Boston Gear DCXplus - DC motion control and RK K Control Coater Model 101
- XRD - AXS D8Focus, with solid state LynxEye detector
- Cell test system - Solartron Analytical 1480 MultiStat

3.2 Chemicals and materials

Table 3.1: The chemicals and materials used

Chemical/Material	Formula	Manufacturer
Carbon nanocones	C	Kværner
Carbon, SLP30	C	Timcal
Kynar, Polyvinylidene fluoride	$(CH_2\text{-}CF_2)_n$	Arkema
N-Methyl-2-pyrrolidone	C_5H_9NO	Aldrich
Lithium hexafluorophosphate	$LiPF_6$	Aldrich
Diethyl carbonate	$C_5H_{10}O_3$	Aldrich
Ethylene carbonate	$C_3H_4O_3$	Aldrich
Trilayer PP/PE/PP	$(CH_2\text{-}C[CH_3]H)_n/(CH_2\text{-}CH_2)_n$	Celgard
Copper	Cu	Circuit Foil
Lithium	Li	Alfa Aeser

Figure 3.1: A slurry which is not done milling. It has not gotten the desired viscosity. [Photo: Morten Onsrud]

3.3 Slurry mixing

The initial experiments focused on finding the optimal mixture for the slurry. The contents of the slurry were polyvinylidene fluoride (PVDF), carbon nanocones (CC), and N-Methyl-2-pyrrolidone (NMP). The PVDF and carbon cones were added at a mass percent ratio of 5:95, respectively. This content was then tested with different mass variation of the NMP, shown in table 3.2.

All the work with NMP was done inside a fume hood. For the first slurry, all the components were mixed with a magnet stirrer prior to being put in the ball milling jar. For the 11th and 13th slurry the PVDF and NMP were mixed with a magnet stirrer inside a fume hood prior to being added in the ball milling jar together with carbon nanocones. For all other slurries the components were put directly in a 500 *ml* alumina ball mill jar. 5 alumina balls with a diameter of 30 *mm* were used for milling the components, as shown in figure 3.1. Different milling times were used to test the effect of milling on viscosity, as well as making sure the mixing was done properly. The speed of the milling was usually 150 rpm, but 250 rpm was also used.

Figure 3.2: This is the tape caster with a doctor blade used in the project. [58]

After the ball milling was finished, the slurry was transferred to a Büchner flask, and evacuated with a water jet pump for one to two hours. This will remove the air bubbles that have been

Slurry no.	CC mass [g]	PVDF mass [g]	Total NMP mass [g]
1	9.51	0.51	50.40
2	9.51	0.52	45.00
3	9.51	0.52	35.01
4	9.50	0.50	29.96
5	9.51	0.51	29.57
6	19.00	1.01	60.01
7	9.51	0.50	30.01
8	9.50	0.50	29.50
9	9.50	0.50	29.00
10	9.50	0.50	28.51
11	9.51	0.50	29.00
12	9.50	0.50	25.01
13	9.50	0.50	25.00
14	9.50	0.50	26.98
15	9.50	0.50	28.00
16	9.50	0.50	29.00
17	9.50	0.50	29.00
18	9.50	0.50	28.01
19	9.50	0.50	29.01
20	9.50	0.50	27.00

Table 3.2: The mass composition of all the carbon nanocone slurries made.

Slurry no.	SLP30 mass [g]	Carbon black mass [g]	PVDF mass [g]	NMP mass [g]
21	13.89	0.36	0.75	30.00

Table 3.3: The slurry made of standard carbon anode material, SLP30, to use as a comparison to the other results.

mixed in the slurry during the ball milling.

Rheology measurements were performed on slurry 16 and 17. Measurements of NMP, NMP with PVDF, and NMP with carbon nanocones were also performed. The latter three had the same mass ratios of the components as slurry 16.

A slurry of commercially available graphite anode material was prepared with the masses shown in table 3.3. This was made the same way as the other slurries, by putting all the components directly into the milling jar without any premixing with a magnet stirrer.

Slurry 6 was made with the double amount of mass that was used in slurry 5. This was to see if the total mass had any effect on the milling time and viscosity.

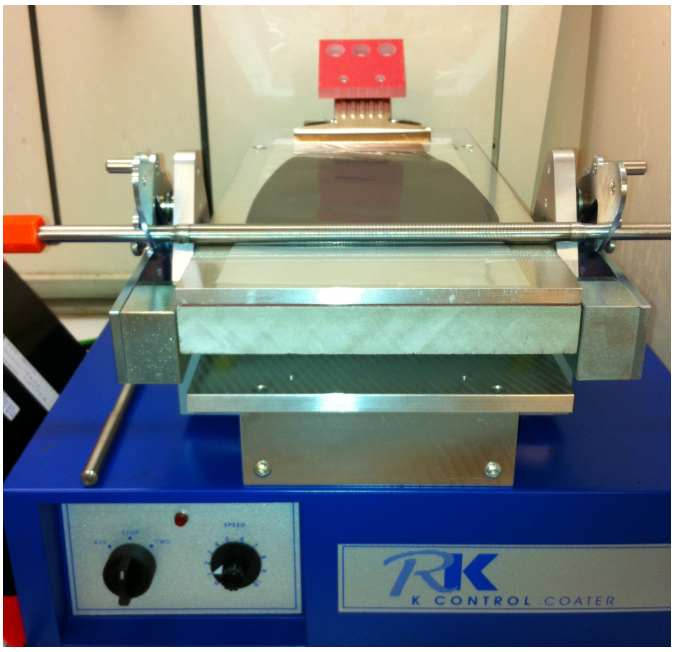

Figure 3.3: This is the tape caster using the coating bars, just after the casting is finished. [Photo: Marius Uv Nagell]

3.4 Slurry characterization

3.4.1 Evaporation

Slurry was poured onto a watch glass and placed on a scale. The weight was measured every 30 minutes to one hour. This was continued for 26 hours, with exception of 15 hours during the evening and night.

3.4.2 Water and ethanol reaction

Small amounts of slurry were added to water. A mixture of NMP and PVDF was also added to water. The mixture of NMP and PVDF was also added to 96 *vol%* ethanol.

3.5 Tape casting

The slurries were tape casted onto copper films using two different tape casters, one with a doctor blade, figure 3.2, and one with spirally wound coating bars, figure 3.3.

3.5.1 Tape casting with doctor blade

The tape caster with doctor blade used a plastic film to extrude the slurry from the doctor blade, as shown in figure 3.4. The doctor blade was rigid and the plastic film was pulled under the copper foil. The copper foil was attached to the plastic film so that the slurry was casted onto the copper rather than the plastic. The speed was varied from 20 to 100% of 20 cm/min. Usually a speed of 20% of 20 cm/min was used.

After the film was casted, it was dried at 83°C on a hot plate with air flow.

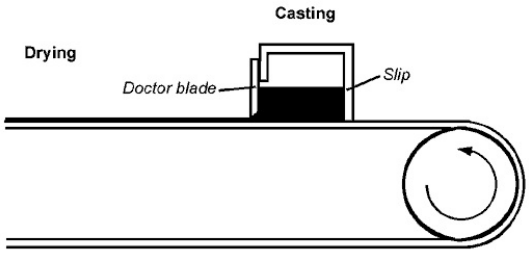

Figure 3.4: A figure which shows the principle of tape casting. Here with a doctor blade [59].

3.5.2 Tape casting with a coating bar

The tape caster with a coating bar used replaceable bars which moved over a stationary plate. A plastic film was attached to the plate, and the copper film was attached to the plastic. Speed of the caster was set to 1. This would be around 2 m/min of the variable speed between 2 and 15 m/min.

After the film was casted, it was dried at 60°C on a hot plate inside a fume hood for two hours.

When the film was finished drying, it was put in a vacuum oven at 120°C overnight to remove remaining moisture and solvent. The thickness of the film was measured after the drying process .

3.6 XRD and SEM of cast

Sections of the casts were removed from the copper foil. These coarse powders were analyzed using X-ray diffraction and compared with results from carbon nanocone powder results.

Casts were also investigated using a scanning electron microscope (SEM). The magnification made it possible to look at cones and other particles in the cast. Looking for damaged particles due to the milling process and patterns from the coating bar were the main reasons for using the SEM.

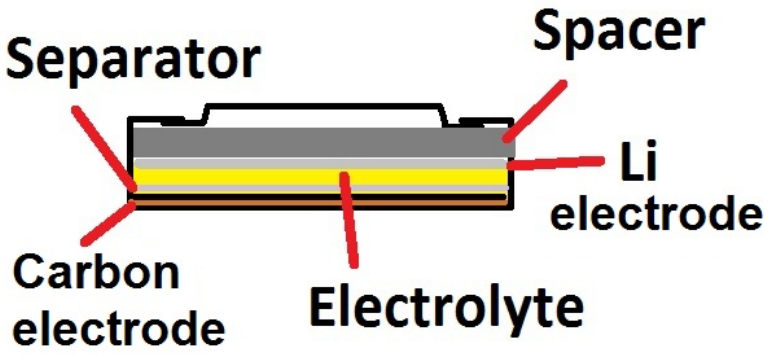

Figure 3.5: Schematic of the assembly order for the coin cells used.

3.7 Electrolyte

The electrolyte used in the batteries was 1 *M* lithium hexafluorophosphate ($LiPF_6$). The salt was added to a solution of 1:1 (%vol) ratio of ethylene carbonate (EC) and diethyl carbonate (DEC) so that the concentration was 1 *M*. The EC needed to be heated up to above 35°C and then DEC was added while stirring with a magnet stirrer. $LiPF_6$ was added to the solution and stirred until all the salt was dissolved. The electrolyte was kept in small glass flasks with screw caps. All the work was done inside a glove box.

3.8 Battery assembly

When the carbon nanocone film was finished drying, it was moved to a glove box with an argon atmosphere. In this glove box the oxygen and water content was held below 0.1 ppm.

The batteries assembled were CR2016 button cells, which mean that the total height of the battery was 1.6 *mm* and the diameter of the battery was 20 *mm*. Figure 3.5 shows the assembly order of the different components.

This project used lithium as a reference electrode, which makes the batteries reference cells. In regular lithium ion batteries the carbon is defined as the anode because the lithium in the carbon structure oxidizes upon discharging. In this project the lithium becomes the anode as upon discharging the lithium oxidizes and the lithium ions intercalate in the carbon. The batteries made in the project also have a potential when assembled, whereas ordinary lithium ion batteries would need to be charged before they get a high potential.

3.9 Battery characterization

The batteries were placed into a battery holder. The batteries were charged and discharged with a potentiostat. The batteries were exposed to different charging and discharging cycles, starting with a slow charging process before faster cycles were initiated.

Coating bar	27.00 g NMP	28.00 g NMP	29.00 g NMP
100 μm	Battery	Battery	Battery
80 μm	Battery	Battery	Battery
60 μm	Battery	Battery	Battery

Table 3.4: Matrix of battery data. In chapter 4.5 the battery parallels are filled in.

The following charge and discharge rates were used. The initial charging was performed in two steps, a charge rate of 10 mA/g was used to reach 0.05 V, before a last charging step of 5 mA/g was used to reach 0.04 V. The first discharge was done with a rate of 20 mA/g until 1.5 V was reached. The rest of the cycles were performed with charge and discharge rates of 40 mA/g. The charge and discharge were terminated at 0.05 and 1.5 V, respectively.

The characterization was planned to be represented in a matrix of three different casted thicknesses and with three different amounts of NMP used in the slurries. The matrix could then easily present the data and determine the significance of the two variables. The proposed matrix is shown in table 3.4

Chapter 4

Results

4.1 Initial slurry experiments

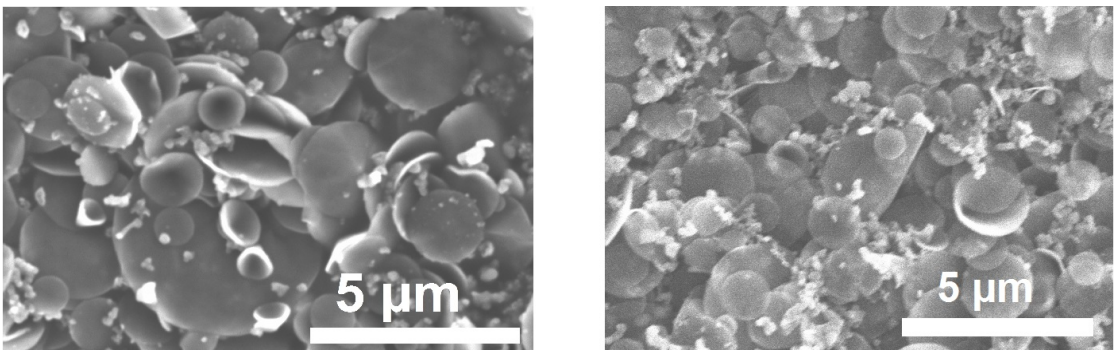

Figure 4.1: SEM images of untreated carbon powder (left) and the cast of slurry 14 (right).

During initial experiments with the slurries the results showed that the particles were not affected by milling time. This can be seen from the fact that after milling slurry 7 for 19 hours and 50 minutes, the viscosity was unchanged compared to only 40 minutes of milling. Figure 4.1 shows that there is no visible difference in the SEM images taken of slurry 14 (16 hours and 50 minutes of milling) and the untreated powder. A low viscosity was maintained for 45 hours in the milling jar with the lid on. The mixture looked like it had maintained its homogeneity.

The optimal mass of NMP was found to be in the range between 25.00 to 30.00 g, based on the casting results and the behavior of the slurries.

The result from a simple evaporation test with a watch glass on a scale is shown in figure 4.2. After this experiment was done, the slurry had developed a film on the surface. This prevented the slurry from running off the watch glass when the it was tilted.

The water and ethanol experiments resulted in polymerization of the PVDF. Both the slurry and NMP/PVDF mixture polymerized when it came in contact with both water and 96 *vol%* ethanol.

4.1.1 The point of viscosity change

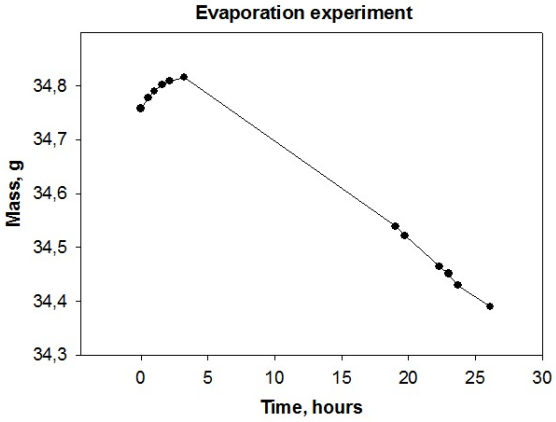

Figure 4.2: The graph of the evaporation test, which shows that the mass is increasing for a couple of hours before decreasing.

The slurries had a point of change in appearance. At some point in the milling process it went from exhibiting very high viscosity to very low viscosity. This is referred to as *the point of viscosity change*. This point appeared during milling intervals. For instance a viscous slurry that had already been milled for some time, was set to mill for 20 minutes. This slurry then got a reduced viscosity during the 20 minutes of ball milling. This also is mentioned in appendix A.1. The point of viscosity change is used as a reference to whether the slurry is properly mixed or not. The reason for this is that all the slurries ended up reaching past this point. Before reaching this point the viscosity was very unpredictable. Increasing milling speed decreased the milling time needed to reach this thinning point.

4.2 Rheology measurements

The rheology of the slurries was measured. The results showed a complex behavior of slurry viscosity, as shown in figure 4.4.

The measurements of the single components showed that the NMP was a Newtonian fluid. 14.50 g of NMP mixed with 0.25 g of PVDF was Newtonian too. 29.00 g of NMP mixed with 9.50 g of carbon nanocones which was ball milled for 13 hours, and showed a shear thinning property down to a point where it became shear thickening. All three compositions are shown in figure 4.5. The viscosity of the NMP was 1.86 $mPa \cdot s$, and for the NMP with PVDF it was 10.7 $mPa \cdot s$. In comparison the viscosity of water at room temperature is approximately 1 $mPa \cdot s$ [54], which also was the observation of measurements done with the rheometer.

Figure 4.3: The slurry was contracting on the plastic film during tape casting with the doctor blade.[Picture: Morten Onsrud]

For slurry 16 and 17 a time dependent viscosity measurement was done for two different

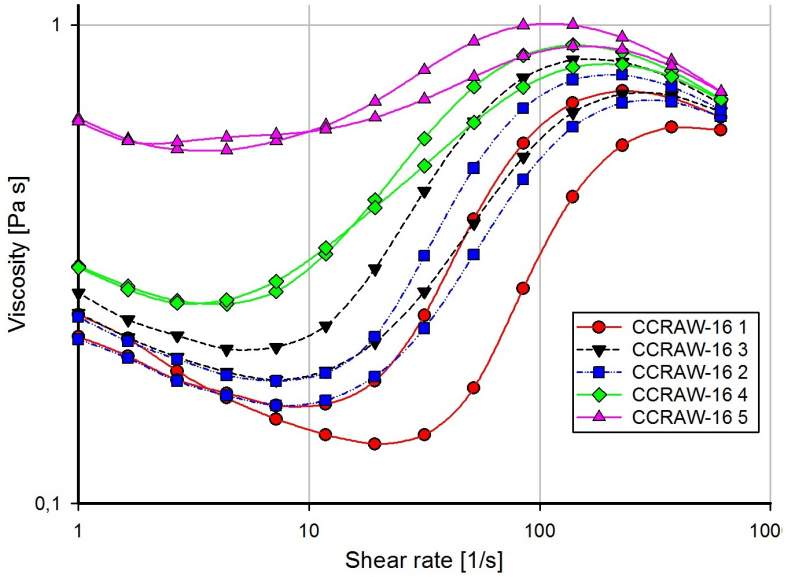

Figure 4.4: The first 5 viscosity results for slurry 16. This shows the tendency for all the slurry viscosities.

share rates. Figure 4.6 and 4.7 shows the results of these measurements. The behavior of the viscosity for the two shear rates is quite different. At high shear rate (1000 s^{-1}), the viscosity is relatively constant, with a slight increase over time. For the low share rate (0.1 s^{-1}), on the other hand, the viscosity is increasing rapidly after 15-20 minutes.

4.3 Tape casting

The low viscosity slurries did not wet the plastic film, as figure 4.3 shows. Less viscous slurries exhibited poorer wetting properties on the plastic than the more viscous ones. A significant difference between the two tape casters was also observed. The tape caster with the casting bar did not have significant amounts of contraction.

Films casted with the tape caster using a coating bar instead of a doctor blade showed almost complete wetting of the slurry. These films showed stripes in the cast, visible to the naked eye. It seemed that the patterns were made by the wound coating bars. There were no visible height differences except for one cast. The thinnest cast from slurry 18 exhibited a rougher surface. The coating bar had clearly made grooves in the surface.

4.4 XRD and SEM characterization of the cast

XRD was performed on casts from slurries 14 and 17, which were milled at 150 rpm and 250 rpm, respectively. The results can be seen in figure 4.8.

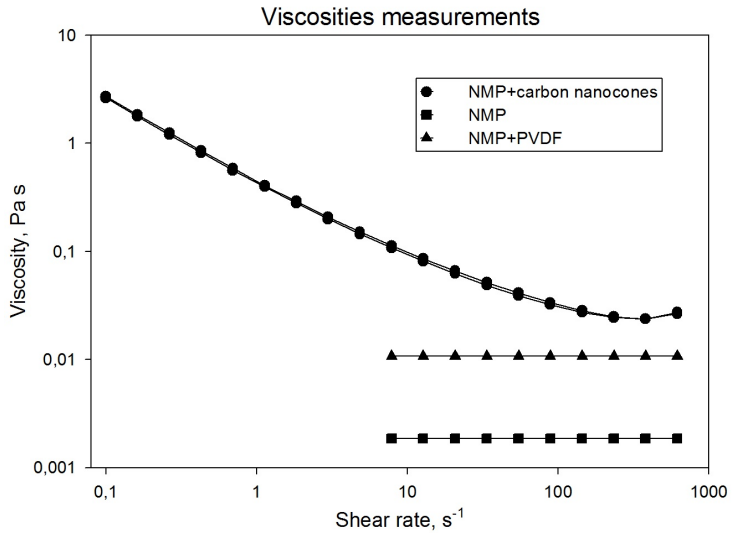

Figure 4.5: The viscosity of NMP, NMP+PVDF and NMP+carbon nanocones.

The casts with the visible stripes were investigated further in a SEM. They were also visible on the SEM images, as shown in figure 4.9.

The thickness of different films is presented in table 4.1.

Slurry no.	Caster	Casting speed, cm/min	Total film thickness range, μm
6	Doctor blade	5	120-139
6	Doctor blade	10	120-127
6	Doctor blade	15	120-125
6	Doctor blade	20	123-127
14	Wound coating bar, 100 μm	200	68-73
15	Wound coating bar, 100 μm	200	68-75

Table 4.1: A table of the measured thicknesses of casted films.

4.5 Battery characterization

The thickness of the anodes that were used in the batteries was measured and is presented in table 4.2. The anodes were all casted with the tape caster that used the coating bar.

Batteries were tested, and results were obtained from all batteries except casts made with the 60 μm coating bar from slurry 18 and 20, due to some technical incident with the program used. Batteries were given names of the following structure CCRAW-cast number-battery number.

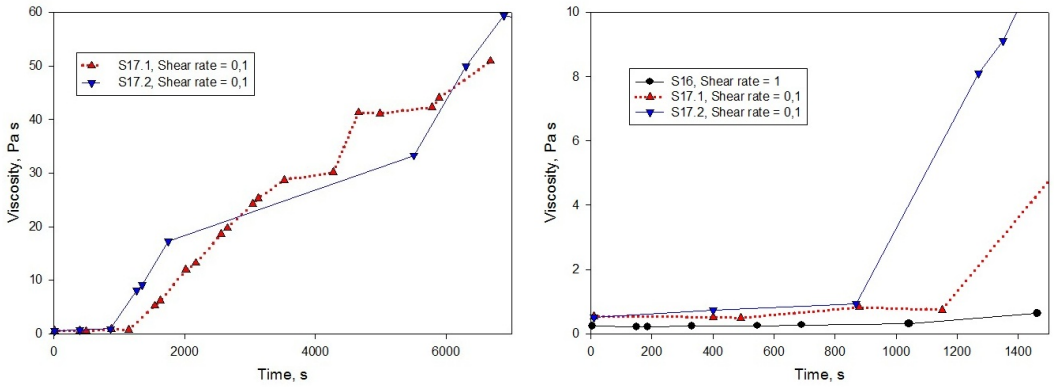

Figure 4.6: The time dependence of the viscosity for the shear rate of 0.1 s^{-1} for slurry 16 and 17. Slurry 17 was tested two times. The right figure is a close up of the left one and also contains the results for slurry 16. The left figure is only results for slurry 17.

The CCRAW indicates that the carbon nanocone used have not been pretreated in any way. CLSP30, instead of CCRAW, indicates that the carbon used for this battery is the SLP30 carbon, a standard commercial carbon material for use as active material in anodes.

Table 4.4 shows the obtained data of all the tested batteries that worked properly.

The data from the first charge/discharge cycle can be seen in figure 4.10, 4.11 and 4.12. These figures compare the data obtained using the 100 μm coating bar and the 80 μm coating bar for the tape casting and data obtained for varying thickness, but with the same amount of NMP. In table 4.3 the data obtained during the project is placed according to the matrix mentioned in chapter 3.9.

The CSLP30-21-1 is included as a reference in all three figures. The full charge/discharge cycles are found in appendix B.1. There is good consistency and stability of the cycle capacities as they do not decrease much for each cycle. No long term cycling has been performed, and so only initial capacity has this far been established.

The irreversible capacity loss of the first cycle, in percentage of its first charge capacity, is plotted against the mass loading (mass per area), and shown in figure 4.13. It is compared to results obtained by Ng *et al.* [11] using TIMREX SLX50 carbon. The carbon cones have high irreversible capacity and lower mass loading compared to both the SLP30 and SLX50. The SLP30 is the two points to the lower right of figure 4.13b.

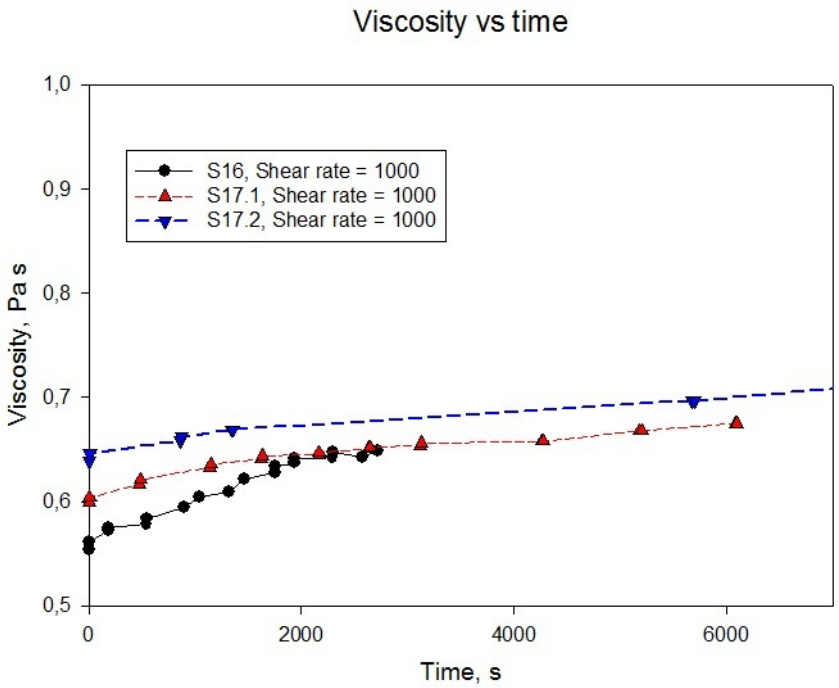

Figure 4.7: The viscosity change over time for the shear rate of 1000 s^{-1} for slurry 16 and 17. Slurry 17 was tested two times.

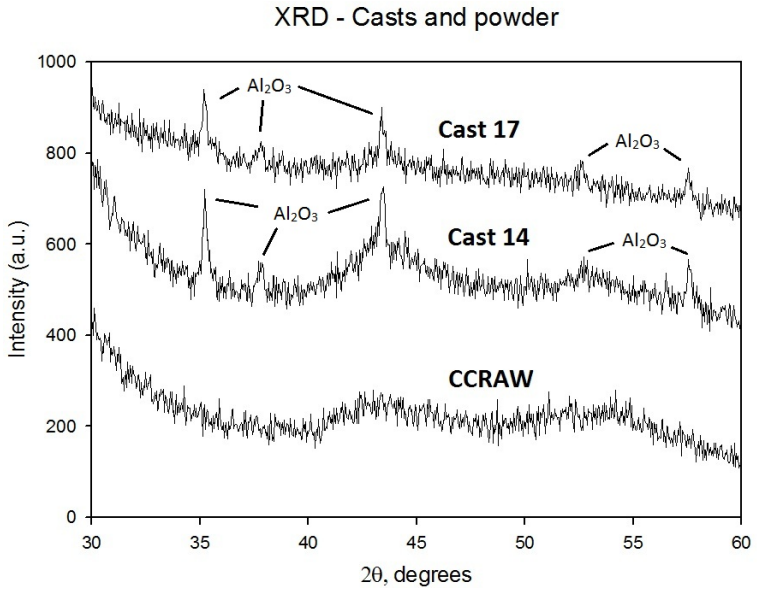

Figure 4.8: The XRD results from the casts of slurry 14 and 17 as well as untreated carbon nanocone powder.

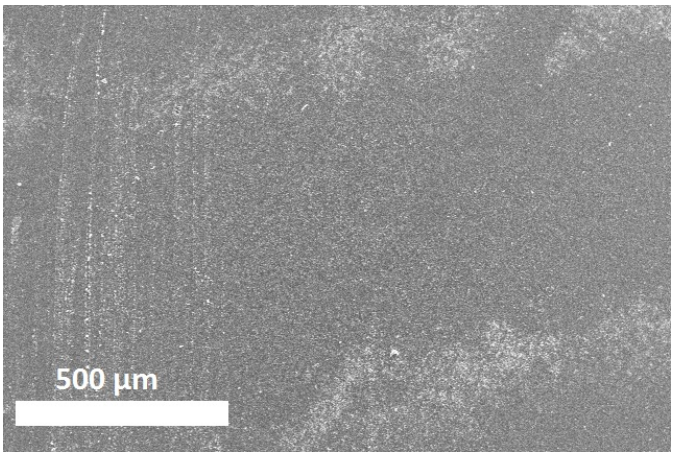

Figure 4.9: SEM image of white, diagonal stripes on the cast of slurry 14, which were also visible with the naked eye.

Slurry no.	Coating bar used	NMP mass, g	Anode thickness, μm (Cu+CC)
14	100 μm	26.98	67-72
15	100 μm	28.00	66-68
16	100 μm	29.00	55-62
20	80 μm	27.00	52
18	80 μm	28.01	50-53
17	80 μm	29.00	52-53
20	60 μm	27.00	43-44
18	60 μm	28.01	47-48
19	60 μm	29.01	38-39
21 (SLP30)	100 μm	30.00	73-75

Table 4.2: A table of the measured thicknesses of the anodes used.

Coating bar	27.00 g NMP	28.00 g NMP	29.00 g NMP
100 μm	CCRAW-14	CCRAW-15	CCRAW-16
80 μm	CCRAW-20.1	CCRAW-18.1	CCRAW-17
60 μm	No data	No data	CCRAW019

Table 4.3: The complete matrix from chapter 3.9 based on the data obtained.

Batteries	Loading, mg/cm^2	1st Charge Capacity	Irreversible capacity loss	Open circuit voltage	Columbic efficiency (%)	1st Cycle Irreversible capacity loss (%)
CCRAW-14-1	2.5987	680	309	2.29	54.5	45.5
CCRAW-14-2	2.8822	708	307	1.64	56.6	43.4
CCRAW-14-3	2.8350	700	313	2.02	55.3	44.7
CCRAW-14-4	2.9294	695	309	1.61	55.5	44.5
CCRAW-14-5	2.7877	779	350	2.40	55.0	45.0
CCRAW-15-1	3.7327	504	222	1.96	55.9	44.1
CCRAW-15-2	3.7800	503	226	3.11	55.1	44.9
CCRAW-15-3	4.0162	479	219	3.13	54.2	45.8
CCRAW-15-4	3.6854	505	229	3.17	54.6	45.4
CCRAW-16-1	2.5987	667	287	1.63	57.0	43.0
CCRAW-16-2	3.0239	665	295	1.69	55.6	44.4
CCRAW-16-3	2.8822	711	314	1.88	55.8	44.2
CCRAW-16-4	2.5515	652	285	1.77	56.3	43.7
CCRAW-17-1	2.1262	740	330	2.08	55.4	44.6
CCRAW-17-2	2.0790	781	357	1.94	54.2	45.8
CCRAW-18.1-5	2.2680	684	307	2.40	55.1	44.9
CCRAW-19-1	1.6537	723	324	3.04	55.1	44.9
CCRAW-19-2	1.7955	669	309	2.52	53.9	46.1
CCRAW-20.1-1	2.3152	670	301	1.78	55.1	44.9
CSLP30-21-1	4.0529	524	96	1.27	81.7	18.3
CSLP30-21-2	4.1910	521	99	3.25	81.0	19.0

Table 4.4: Numbers from the first charge/discharge cycle.

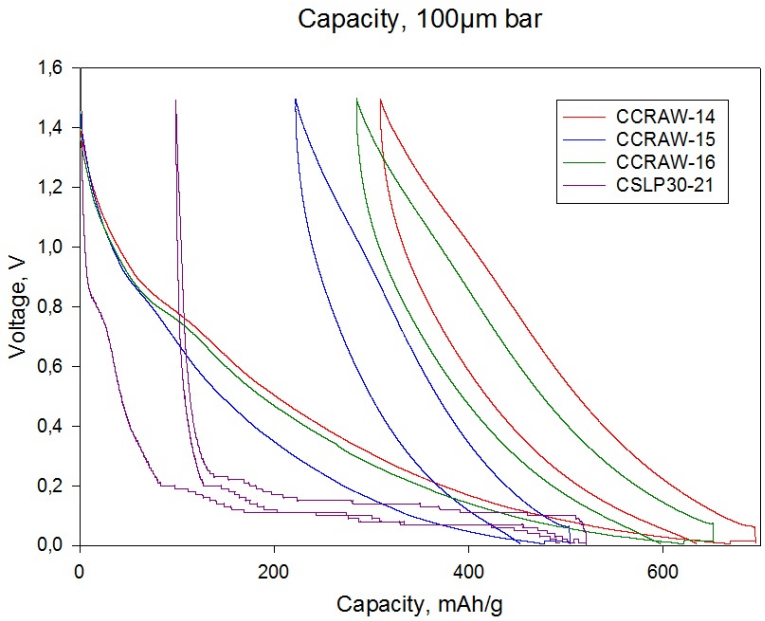

Figure 4.10: This figure shows the first charge and discharge, as well as second charge, for CCRAW-14-4, CCRAW-15-1, CCRAW-16-4 and CSLP30-21-2.

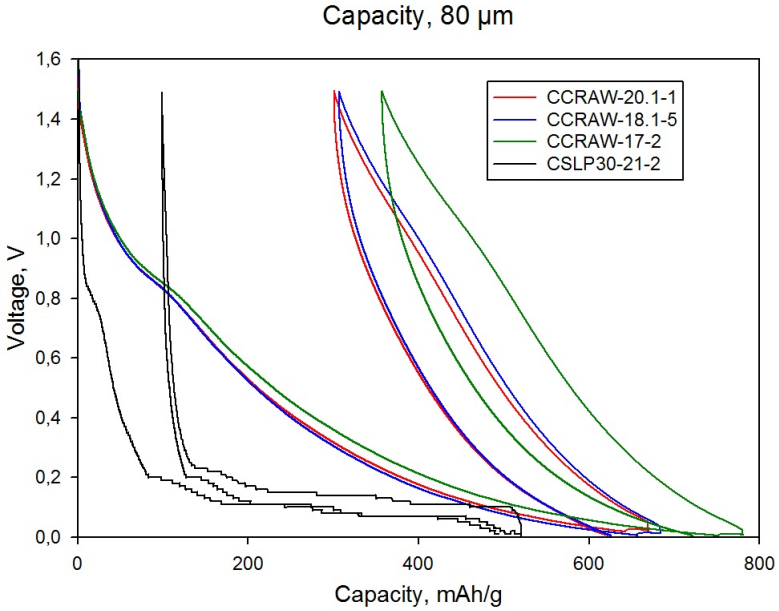

Figure 4.11: This figure shows the first charge and discharge, as well as second charge, for CCRAW-18.1-5, CCRAW-20.1-1, CCRAW-17-2 and CSLP30-21-2.

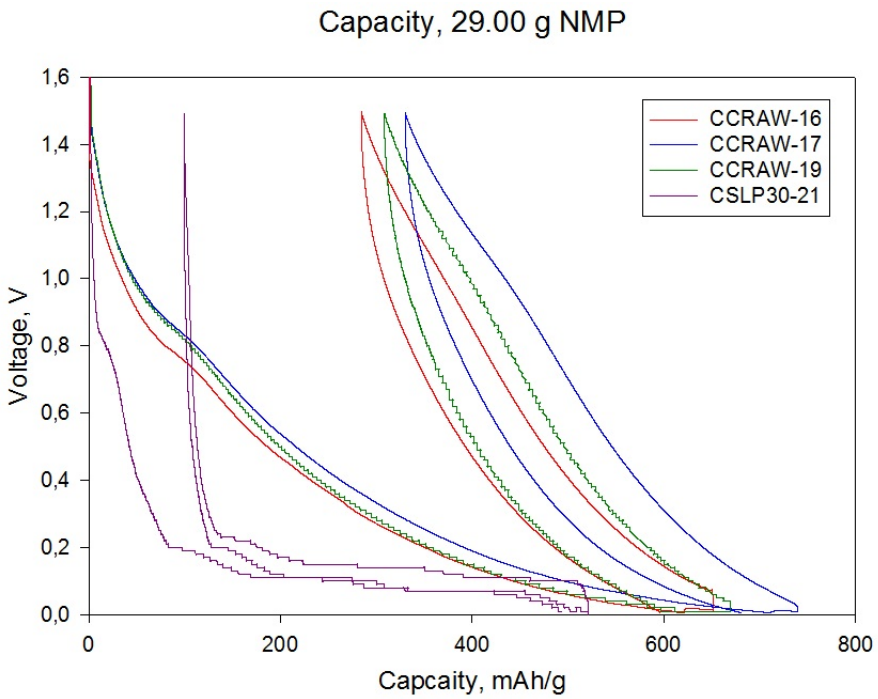

Figure 4.12: This figure shows the first charge and discharge, as well as second charge, for CCRAW-16-4, CCRAW-17-2, CCRAW-19-2 and CSLP30-21-2. They had varying thickness.

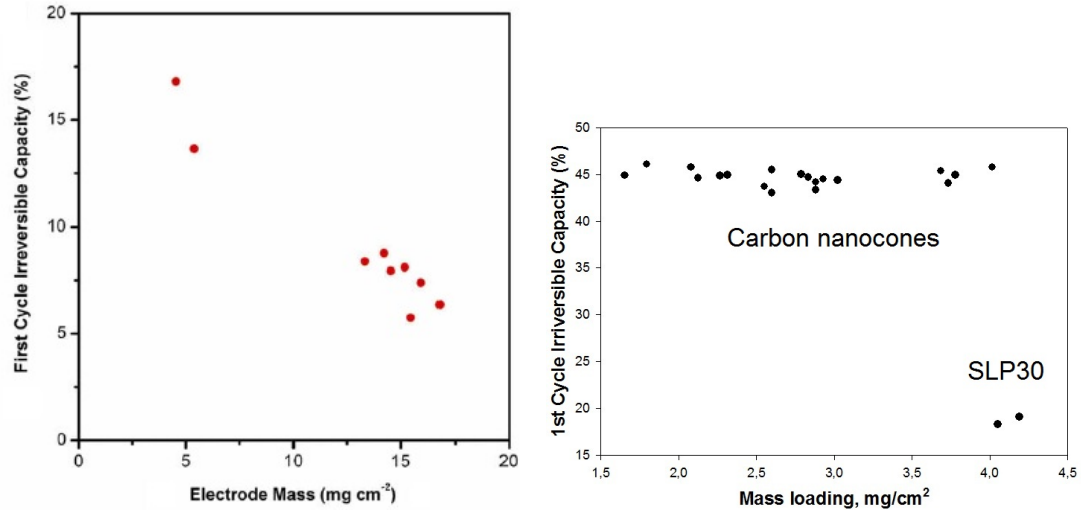

(a) Results by Ng *et al.* [11]

(b) The results of this project.

Figure 4.13: The irreversible capacity versus the mass loading.

Chapter 5

Discussion

5.1 Initial slurry experiments

The first six slurries made were used to find a proper viscosity for the doctor blade tape caster. Viscosity and wetting behavior observed during casting indicated that the optimal ratio of PVDF and carbon nanocones to NMP would be between 1:2.5 and 1:3. Two variables that appeared to be of importance were the total milling time and the procedure of adding NMP. By adding NMP in between the rounds of milling the result for slurries with the same weight ratios were equal. Slurry 4, 6, and 7 had approximately the same ratios, 1:2.990, 1:2.999, and 1:2.998 respectively. They had different milling times and procedures of adding NMP, as described in appendix A.1. The total mass was also different, as slurry 6 had double the mass of slurry 4 and 7. The results of this could indicate that the total mass could affect the results of the mixing time, although this was not further tested. It was used more as an indicator of the possible importance of keeping the mass of the carbon cones and PVDF constant.

One evaporation test in air, on a scale was done, and it showed increase in weight during the first couple of hours. This weight increase is most likely due to reactions with water evaporation in the air. After a while the weight began to decrease. This was due to evaporation of NMP. The final result, after almost 26 hours, was a film which seemed to have reacted with water in the air. It hindered the slurry from running off the watch glass when it was tilted, as figure 5.1 shows. The film must have consisted of polymerized PVDF. Tests done with PVDF and NMP solutions showed that the solution polymerized into a gel looking substance when exposed to water. Even adding 96 *vol%* ethanol made the solution to polymerize. Both these experiments show that PVDF reacts with water. This means that it is important to prevent the slurry from being exposed to air over longer periods of time. The exposure to air can destroy the quality of the slurry.

5.1.1 The point of viscosity change

Variations in viscosity, or lack thereof, showed that the particles were not destroyed during ball milling. If the particles had been destroyed or made smaller, the slurry would have become more viscous after long milling periods. This is because, as chapter 2.3.1 mentions, the surface area

Figure 5.1: The watch glass with the slurry after about 27 hours of air exposure. [Photo: Marius Uv Nagell]

of the particles increase, thus creating more friction between the particles. Evaporation of NMP have the same effect, but slurry 7 was left for 45 hours after the final round of milling, with a lid on. The slurry still looked as it did after 40 minutes of milling, so evaporation was not a problem.

Sedimentation of the slurry did not seem to be a problem either, as no visual inhomogeneity was observed. This indicates that when the slurry turns into a less viscous mixture it is likely that the precursors are well mixed and have become homogenous.

The thinning point could be a reason for inconsistent results for different slurries. The fact that there is a certain point which makes the slurry become less viscous, can be the reason for the different viscosities obtained for the different milling times of slurry 4, 6, and 7.

The milling time needed to reach the point of viscosity change was investigated with slurry 8, 9 and 10. Three different ratios were milled for times based on earlier attempts, which were thought to have been sufficient to reach this point. There was a distinct difference in milling time for just a small change of mass of NMP. By decreasing the amount of NMP from 29.5 g to 29.0 g the milling time went from 60 to 90 minutes. Further decreases made the time increase further. Slurry 12, with 25.00 g NMP, did not reach the thinning point even after 6 hours of milling. Another 12 hours, 18 hours in total, was needed for it to finally pass the point of viscosity change. This change in time required to reach the point of viscosity change were thought to be because of the NMP, but later results indicated that the milling speed could be the decisive factor.

Premixing the PVDF and NMP decreased the milling time of slurries with 29.0 g NMP from

90 to 60 minutes, but premixing itself took over two hours. Since reduction in milling time did not reduce the total time used to make the slurry, therefore the premixing process was dismissed. The later mixing processes were done overnight, for 12 to 18 hours.

SEM images confirmed the viscosity observations, which showed that milling over a long period of time did not destroy the carbon nanocones (see figure 5.2). This could indicate that the carbon nanocones also could be unaffected by increasing the ball milling speed. A higher milling speed was investigated to see if it could decrease the milling time. Due to technical problems with the equipment, the milling of slurry 17 did not start and the content was left in the jar overnight. This was followed by 15 minutes of milling at 250 rpm. This made the slurry reach the point of changed viscosity.

The sound that the ball made during the 250 rpm milling suggests that 250 rpm is a more effective mixing speed for the slurries. This is based on the fact that the balls made more noise for the slurry with low viscosity, compared to higher viscosity. A more viscous slurry impairs the movement of the balls and the ball milling is not as efficient while milling at 150 rpm, as it is at 250 rpm. At 250 rpm the balls make an even, rolling sound as they seem to roll around against the walls and performing an effective mixing.

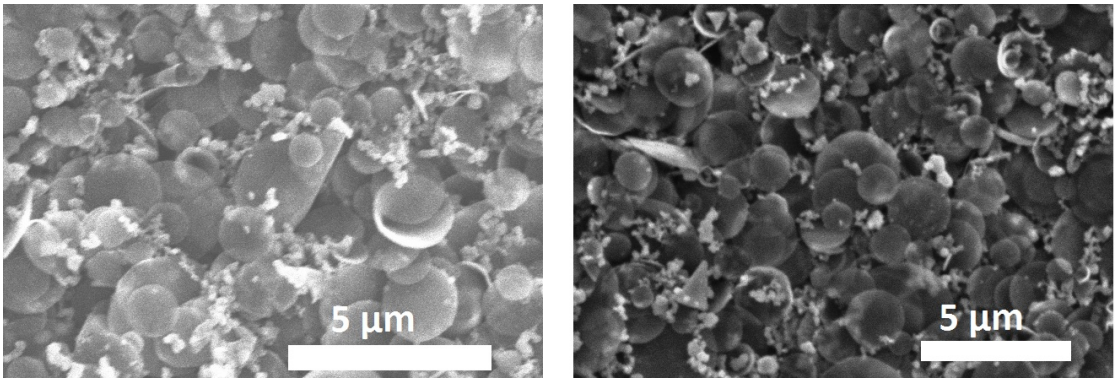

Figure 5.2: SEM images of the casts of slurries 14 (left) and 17 (right). No severe damage can be seen.

5.2 Rheology measurements

The complex viscosities of the slurries are due to the interaction between carbon and the binding polymer, PVDF. The viscosity changed as a function of time and shear rate. This indicates that it is not a Newtonian fluid.

Rheological measurements of the components of the slurry, NMP, NMP and PVDF, and NMP and carbon nanocones, were done. They did not explain the behavior of the slurries. On the other hand, these measurements could indicate that the carbon and PVDF interactions that Yoo *et al.* [57] found can explain the behavior observed here. As Yoo *et al.* observed that PVDF and carbon made hydrogen bonds with each other, creating a complex system of carbon and PVDF. They found out that the higher the viscosity, the more homogenously dispersed the

PVDF was in the slurry. This reltaion can explain the increase in the viscosity at low share rates. The geometry of the cones and discs can also be one of the reasons for the strange behavior of the slurry. The cones and the discs might lead to creation of more complex fluid systems than ordinary particles which are more round in their shape.

When the milling balls were taken up from the milling jar, the slurry started dripping from the balls. These droplets were long and elastic. This is an indicator that the slurry has viscoelastic properties. The viscoelastic behavior of the slurry could originate from the PVDF-carbon interactions. Interactions would make hydrogen bonds between the polymers and cones, which would give a more viscous fluid. The point from where the slurry goes from viscous to a less viscous could indicate that the PVDF is becoming more evenly dispersed. The slurry might have gone from a regime with larger agglomerates with high friction, to well dispersed discs and cones in a solvent.

The hysteresis loops of the viscosities could look like those of thixotropic and rheopectic fluids. The results from the low shear rate to the high shear rate is the lower curves, and the high curves, in the same color, is from the high to low shear rates. The hysteresis loop indicates the energy needed to destroy the network of polymer-particle bonds. This seems to increase, meaning that the bonds become more evenly dispersed for every time they are torn apart. This viscosity change could also partially derive from the fact that the slurry reacts with evaporated water in the air. This means that the exposure to air should be kept to a minimum.

The relatively constant viscosity at high shear rate would correspond to the viscosity of the individual components of the slurry. This means that when the bonds are broken, the system is free to move more, thus an almost constant viscosity is observed at this rate. The viscosity at low share is changing over time, so it is not a real rheopectic fluid. Increasing viscosity would imply that it is not a real thixotropic fluid either.

The exposure to air has showed that there are reactions happening in the slurry. The reactions can affect the viscosity and make the viscosity increase. These reactions are most likely between water in the air and the PVDF in the slurry. More polymerization would make the polymers larger. This could mean that they can make hydrogen bonds with more carbon nanocones and increase the viscosity. This is the case for the low shear measurements. For the higher shear the viscosity is almost constant. This may indicate that the level of shear needed to destroy the polymer-carbon bonds is less than 1000 s^{-1}.

5.3 Tape casting

Many of the slurries were tape cast in order to observe how the slurries behaved at different viscosities, and find out which viscosities were best for battery purposes. The first films were cast using a doctor blade. Using a doctor blade demands a slurries that are not too little viscous. The slurries are being casted through a slit, which means that the slurry has to be viscous enough to not pour out of the slit. If it starts flowing around, the control of the cast can be lost.

Slurry 1 was tape cast on plastic. The viscosity was too low and ran out from the doctor blade opening. Slurry 1 did not wet the plastic properly, and this could also be due to the low viscosity. The less viscous slurries wetted the plastic less than the more viscous ones. A change in viscosity would possibly change the surface tension of the slurry. In this case, the more

viscous slurries would then have a lower contact angle with the surface than the low viscosity slurries.

The polarity of the plastic film and the NMP would also affect these results. The less viscous the slurry is, the more NMP the slurry contains, and it becomes more polar. More opposing forces would then decrease the wetting and increase the contact angle.

Droplets of slurry 3 were placed on a piece of copper film. The slurry wetted the copper better than the plastic. As the slurry would retract from the plastic to the copper foil, the film thickness would increase on the copper film edges. This was not shown as a problem on later casts.

The initial slurries were made with emphasis on achieving a viscosity suited for the tape caster with the doctor blade. The point of viscosity change gave slurries with lower viscosity compared to the first six slurries. To make more viscous slurries, less NMP is needed. Experiments with NMP and milling time showed that the lower amount of NMP, the longer time it takes for the slurry to reach the point of viscosity change for a milling speed of 150 rpm. This increase in time is not favorable. The tape caster with the coating bar, on the other hand, worked well with the less viscous slurries. Viscosities of the slurries were optimal for the tape caster with the coating bar.

The tape caster with the coating bar used bars with grooves in it. The width and depth of the grooves decided the thickness of the film. The grooves gave visible patterns in the casts. These were visible as light grey stripes on a darker grey surface. The patterns suggest a visible, uneven surface. Observations at various angles, with the naked eye, were done to see if the visible stripes were showing as peaks on the surface, but this was not observed. A smooth, shiny surface was instead observed at lower angles. When thinner grooves were used on the coating bar the surface became visibly uneven to the naked eye. Viscosity measurements might be used to explain this. With thinner grooves in the wound coating bars comes higher shear rate applied on the casted slurries. After the slurry is casted, the applied shear rate is very low. The viscosity at high shear rates were lower than at the low shear rate, meaning that the slurry will run less after the coating bar has been used to cast the film. Rougher patterns during the casting shear will give greater impact on the roughness of the casted film.

5.4 XRD and SEM characterization of the cast

Cast slurries were investigated in an SEM shown in figure 4.1 (in Results) and 5.2. The figures show the carbon nanocone powder and the two casts milled at different milling speeds, 150 and 250 rpm for slurries 14 and 17, respectively. There is no visible difference in the particle size, or any sign of destroyed particles.

The XRD shows no difference between cast 14 and 17. They both have the same peaks at the same 2θ angles. Both casts are different from the raw powder, with some 2θ peaks corresponding to Al_2O_3. This alumina is likely to originate from the alumina powder used to clean the milling jar and balls. There might be traces of alumina in the carbon powder too. Conclusively the results show that faster milling will not affect the particle size. Hence the milling speed will not be a variable that should affect the results. The alumina contamination, on the other hand, can affect the results. A method for reducing the contamination should be

found.

5.5 Battery characterization

The thickness of the cast slurries were uniform across the film, which means that the anode thickness can be controlled. This also gave room for experimenting with different thicknesses to compare the effect of thickness of the anode on the battery performance. The initial charge capacity of the batteries vary from 480 to 780 mAh/g. The highest first charge capacities are achieved by batteries from cast 14 and 17. All the batteries show capacities above the theoretical value for LiC_6, 372 mAh/g.

The CCRAW-14 batteries were the batteries with the highest first charge capacity of the battery anodes tape cast with the 100 μm coating bar. They were also the thickest anodes used. The CCRAW-16 also shows a good first charge capacity, with the thickness 10 to 15 μm lower than the CCRAW-14. Of the anodes tape cast with the 100 μm coating bar, only CCRAW-15 actually stands out, with lower first charge capacity. The reason for this might be the battery assembly process. This is a process performed by humans, and this can cause unintentional differences during assembly. Assembly should not cause these differences but it is a possibility. Incidents earlier in the process could also be a reason. Presence of alumina have been seen, and this sample might be more contaminated that other samples, leading to lower capacity.

The batteries with the anodes tape cast with the 80 μm show a more stable first charge capacity between 670 and 780 mAh/g. Their thicknesses are the same. This might imply that the three different amounts of NMP used, really do not affect the results too much. A lack of quantities of results, like the CCRAW-14 to 16 have, makes this results uncertain. It could be that these results really are representative for their respective anodes, but there are not enough results to really support this. Especially with the uncertainty and spread in results for the CCRAW-14 to 16, it shows that the need for a larger amount than one result per anode parallel is needed.

It would look like the amount of NMP does not really affect the results as much that the difference between 27 and 29 g really does impact the results. The CCRAW-16, 17, and 19 anodes were all made with 29 g NMP. They were all tape cast with different thicknesses on the coating bar; 100 μm, 80 μm, and 60 μm, respectively. The final film is between 55 to 66% of the cast thickness. The thickness of the film does not seem to affect the first charge capacity too much, as it is kept between 650 and 780 mAh/g. CCRAW-17 shows the highest first charge capacities of all the battery anodes made, indicating that anode thickness around 50 to 55 μm is the optimal one. This should of course be validated with more results, but as shown now, that is what the results shows.

The biggest problem for these carbon nanocone anodes is the high irreversible capacity loss between 220 and 360 mAh/g. High irreversible capacity loss is caused partially by SEI that is being formed. Another capacity loss mechanism is lithium ions that get trapped inside the carbon structures. The positioning of the cones and discs can be a local factor of how much SEI is formed. The edge planes are better sites for SEI formation than the basal planes. This would imply that the cones lying with the apex towards the current collector have more edge planes exposed towards the electrolyte than a cone with its apex towards the electrolyte. This can create local differences in SEI formation.

The high irreversible capacity loss gives a low Columbic efficiency for all the batteries. The Columbic efficiency stays around 55% for all the batteries, except for the reference carbon, SLP30. These batteries had a Columbic efficiency of just above 80%, which is substantially better than the carbon nanocones. Amongst the carbon nanocone anodes, the CCRAW-16 shows a slightly better average Columbic efficiency compared to the other anodes. This indicates that the optimal anode parameters to continue to work with would be 29.00 g

of NMP and tape casting with 100 μm. Still, the Columbic efficiencies are very similar, and this would imply that small factors are separating the best from the worst amongst the carbon nanocone anodes.

Another difference from the SLP30 carbon anodes is the behavior of the voltage. The charge/discharge curves, figure 4.10 to 4.12, does not have the same form. The SLP30 curves show a higher loss/gain of the voltage before a stabilization occurs. This phenomenon indicates a high internal resistance. This is more the case for the first charge for the carbon nanocone anodes, compared to the following charge/discharge cycles. The SLP30 anodes maintain this voltage loss/gain behavior more than the carbon nanocone anodes. The carbon nanocone anodes have an even decrease/increase in the voltage upon charge/discharge. The reason that the curves are not more similar to the SLP30 could be because of the high irreversible capacity loss. This is not investigated in this project, and therefor this cannot be confirmed but rather mentioned as it is a distinct difference.

In comparison to the other carbon anodes tested by other research groups, the carbon cones show first cycle capacities that are comparable with the graphene nanosheets (540 mAh/g) [42]. Even the lowest capacity results are above most of the results from hollow carbon shells (325 mAh/g) [44], nanospheres (420 mAh/g) [45], and boron oxide doped hard carbon (394 mAh/g) [43]. This shows that the carbon nano cones can have a potential as an anode material if the irreversible capacity loss is reduced.

Ng *et al.* [11] showed results that indicated that the carbon they used, Timrex SLX50, would get reduced irreversible capacity loss when the mass loading was increased. Compared to Ng *et al.* , the carbon nanocones mass loading is much smaller, and its irreversible capacity loss is also higher. This can be caused by differences in the density of the two materials.

The cycles of every battery showed that the capacity change of the battery did not change much for each cycle. This can indicate that the anode withstands a high amount of cycles. However, there are no long term results to prove this, it is a mere speculation.

Chapter 6

Conclusion

In this project carbon nanocones from Kværner was used as an anode material for lithium ion batteries. The process of making the slurries needed to cast the anode material was thoroughly investigated to find an optimal route which would be repeatable and controllable. Casting of the slurries was done with a tape caster with either a doctor blade or a wound coating bar. Controllability of the film thickness was a main target for these experiments. The result was a slurry that could be reproduced and cast easily. Rheological measurements were also done on the slurries to find its viscosity and rheological properties. These slurries showed complex viscosity behavior, but with properties which would be suited to get nice and even films.

The casts were then made with different thicknesses and with three different slurry compositions, to find the best parameters for use in batteries. Batteries were assembled and tested with charge/discharge cycles. The charge/discharge results showed batteries with high initial charge capacities, 480 to 780 mAh/g, but also with a high irreversible capacity, 220 and 360 mAh/g. High irreversible capacity loss should be avoided, so there lays the problem of the carbon nanocones as an anode material. It also shows lower mass loading compared to commercial carbon materials used as anode material (SLP30, SLX50).

The carbon nanocones shows a great potential as an anode material in lithium ion batteries as it has a good initial charge capacity compared to other results from other research groups. By reducing the irreversible capacity this could become a good anode material.

6.1 Further work

Further work for the carbon nanocone anodes will be to do AC impedance spectroscopy to find the internal resistance of the anode. Surface characterization will also be done with techniques like IR spectroscopy. Characterizing the surface chemistry can be helpful in understanding what could be done to control SEI formation and thereby reduce the irreversible capacity loss. Improving the battery assembly procedure, as well as finding ways to minimize the alumina contamination will also be evaluated.

Other possibilities include treating the carbon nanocone powder at elevated temperatures or with microwaves and look at what effect this pretreatment will have on the final anode material.

Finding alternative additives to improve the anode and reduce the irreversible capacity would also be considered, as well as finding other electrolytes which can be used.

Bibliography

[1] V. A. Sethuraman, L. J. Hardwick, V. Srinivasan, R. Kostecki, Journal of Power Sources 2009, 195, 3655-3660

[2] A. K. Shukla, T. Prem Kumar, Current Science 2008, 94 (3), 314-331

[3] M. Ge, K. Sattler, Chem. Phys. Let. 1994, 220, 192-106

[4] Kværner ASA, patent No. PCT/NO98/00093 for production of micro domain particles by use of a plasma process

[5] A. Krishnan, E. Dujardin, M. M. J. Treacy, J. Hugdahl, S. Lynum, T. W. Ebbesen, Nature 1997, 388, 451-454

[6] J.-M. Tarascon, M. Armand, Nature 2001, 414, 359-367

[7] M. G. Kim, J. Cho, Adv. Funct. Mater. 2009, 19, 1-18

[8] A. Patil, V.Patil, D. W. Shin, J.-W. Choi, D.-S. Paik, S.-J.Yoon, Materials Research Bulletin 2008, 43, 1913-1944

[9] Cameron Motor Works Electric Vehicle Conversion, Battery Physics - EV Physics, August 2004, http://www.cameronsoftware.com/ev/EV_BatteryPhysics.html (09.11.2010)

[10] K. Zaghib, J. Shim, A. Guerfi, P. Charest, K. A. Striebel, Electrochem. Solid-State Lett. 2005, 8 (4), A207-A210

[11] S. H. Ng, C. Vix-Guterl, P. Bernando,N. Tran,J. Ufheil,H. Buqa, J. Dentzer, R. Gadiou, M. E. Spahr, D. Goers, P. Novák, Carbon 2009, 47, 705712

[12] C.-G. Wu, M.-I. Lu, H.-J. Chuang, J. Power Sources 2006, 159 (1), 295-300

[13] T. Xu, W. Wang, M. L. Gordin, D. Wang, D. Choi, JOM 2010, 62 (9), 24-30

[14] D. Choia, D. Wanga, V. V. Viswanathana, I.-T. Baeb, W. Wanga, Z. Niea, J.-G. Zhanga, G. L. Graffa, J. Liua, Z. Yanga, T. Duongc, Electrochem. Commun. 2010, 12 (3), 378-381

[15] L. Sun, C. C. Chan, R. Liang, Q. Wang, IEEE Vehicle Power and Propulsion Conference (VPPC), September 3-5, 2008, Harbin, China

[16] G. T. K. Fey, D. C. Lee, Y. Y. Lin, T. Prem Kumar, Synth. Met. 2003, 139, 71-80

[17] Y. Yishi, T. Nishida, S. Suda, M. Kobayashi, Hitachi Company Technical Report 2006, 47, 29-32

[18] Y. H. Lee, K. C. Pan, Y. Y. Lin, T. Prem Kumar, G. T. Fey, Mater. Cham. Phys. 2003, 82, 750-757

[19] T. Prem Kumar, R. Ramesh, Y. Y. Lin, G. T. K. Fey, Electrochem. Commun. 2004, 6, 520-525

[20] J. Chen, Y. Liu, A. I. Minett, C. Lynam, J. Wang, G. G. Wallace, Chem. Mater. 2007, 19, 3595-3597

[21] Y. Kwon, G. S. Park, J. Cho, Electrochim. Acta 2007, 52, 4663-4668

[22] J.-H. Kim, H.-J. Sohn, H. Kim, G. Jeong, W. Choi, J. Power Sources 2007, 170, 456-459

[23] C. K. Chan, H. Peng, G. Liu, K. McIlwroth, X. F. Zhang, R. A. Huggins, Y. Cui, Nature 2008, 3, 31-35

[24] J. C. Hunter, J. Solid State Chem. 1981, 39, 142-147

[25] A. K. Padhi, K. S. Nanjundaswamy, J. B. Goodenough, J. Electrochem. Soc. 1997, 144, 1188-1194

[26] S. Y. Chung, J. T. Bloking, Y. M. Chiang, Nature Mater. 1, 123-128

[27] D. Aurbach, Y. Talyosef, B. Markovsky, E. Markevich, E. Zinigrad, L. Asraf, J. S. Gnanaraj, H.-J. Kim,

[28] T. Jackson, Lithium, 2007, Marshall Cavendish Corporation, New York, USA

[29] F. Galobardes, C. Wang, M. Madou, Diamond & Related Materials 2006, 15, 1930-1934

[30] S. S. Zhang, Journal of Power Sources 2007, 163, 713-718

[31] S. Iijima, Nature 1991, 354, 56-58

[32] H. W. Kroto, J. R. Heath, S. C. O'Brien, R. F. Curl, R. E. Smalley, Nature 1985, 318, 162 - 163

[33] M. F. Yu, O. Lourie, M. J. Dyer, K. Moloni, T. F. Kelly, R. S. Ruoff, Science 2000, 287, 637-640

[34] X. Lu, Z. Chen, Chem. Rev. 2005, 105 (10), 3643-3696

[35] A. Y. Ganin, Y. Takabayashi, Y. Z. Khimyak, S. Margadonna, A. Tamai, M. J. Rosseinsky, K. Prassides, Nature Matt. 2008, 7, 367-371

[36] K. S. Novoselov, A. K. Geim, S. V. Morozov, D. Jiang, Y. Zhang, S. V. Dubonos, I. V. Grigorieva, A. A. Firsov, Science 2004, 306, 666-669

[37] Class for Physics of the Royal Swedish Academy of Science, Graphene - Scientific Background on the Nobel Prize in Physics 2010, Stockholm, Sweden, http://nobelprize.org/nobel_prizes/physics/laureates/2010/sciback_phy_10_2.pdf (02.12.2010)

[38] J. Muller, A. T. Skjeltorp, G. Helgesen, K. D. Knudsen, H. Heiberg-Andersen, Silicon Versus Carbon, 2009, Springer Nederland, 285-292

[39] n-Tec, Scandinavian Advanced Technology, http://www.n-tec.no (14.12.2010)

[40] H. Heiberg-Andersen, A. T. Skjeltorp, K. Sattler, Journal of Non-Crystalline Solids 2008, 354, 5247-5249

[41] N. Yang, G. Zhang, B. Li, Appl. Phys. Lett. 2008, 93, 243111-1-243111-3

[42] E. J. Yoo, J. Kim, E. Hosono, H.-S. Zhou, T. Kudo, I. Honma, Nano. Let. 2008, 8 (8), 2277-2282

[43] X. Wu, Z. Wang, L. Chen, X. Huang, Solid State Ionics 2004, 170, 117-121

[44] F. Su, X. S. Zhao, Y. Wang, L. Wang, J. Y. Lee, J. Mater. Chem. 2006, 16, 4413-4419

[45] Y. Wang, F. Su, C. D. Wood, J. Y. Lee, X. S. Zhao, Ind. Eng. Chem. Res. 2008, 47, 2294-2300

[46] V. G. Khomenko, V. Z. Baruskov, Electrochem. Acta 2007, 52, 2829-2840

[47] M. Yoo, C. W. Frank, S. Mori, S. Yamaguchi, Chem. Mater. 2004, 16, 1945-1953

[48] M. Yoo, C. W. Frank, S. Mori, Chem. Mater. 2003, 15, 850-861

[49] G. Park, H. Nakamura, Y. Lee, M. Yoshio, J. Power Sources 2009, 189, 602-606

[50] D. Capozzo, S. Fleming, B. Foley, M. Macri, Lithium Ion Battery Safety, December 2006, U.S. Consumer Consumer Product Safety/Worchester Polytechnic Institute

[51] X. M.Wang, E. Yasukawa, S. Kasuya, J. Electrochem. Soc. 2001, 148, A1066-A1071

[52] Celgard Microporous Membranes, Celgard Overview Borchure, Celgard.com, http://www.celgard.com/pdf/library/Celgard_Overview_Brochure_10003.pdf (02.12.2010)

[53] Prof. J. A. Nairn, Chapter 6 - Viscosity, Polymer Characterization, 2003, Material Science & Engineering 5473, http://www.scribd.com/doc/3239925/45/Viscosity-Summary (04.12.2010)

[54] W. D. Callister, Jr., D. G. Rethwisch, Chapter 12 - Structure and Properties of Ceramics (pp. 450), Materials Science and Engineering - An Introducion, 2007, John Wiley & Sons, Inc., New York, USA

[55] A. J. Frank, Understanding Rheology of Structured Fluids, 2004, AAN016, TA Instruments, Delaware, USA

[56] R. D Sudduth, J. Applied Polymer Science 1993, , 48 (1), 25-36

[57] M. Yoo, C. W. Frank, S. Mori, Chem. Mater. 2003, 15, 850-861

[58] H. L. Lein, T. Tezuka, T. Grande, M.-A. Einarsrud, Membranes and fuel cells based on proton conducting oxide materials, FUNMAT meeting 2007, http://filer.funmat.no/FUNMAT_meeting_2007/FOETsession/Lein.pdf (07.12.2010)

[59] Breviary Technical Ceramics, From Powder to Part - 4.1.3 Forming, http://www.keramverband.de/brevier_engl/4/1/4_1_3.htm (11.12.2010)

Appendix A

Slurries

A.1 Milling process and casting details

The slurries were milled and casted. Here is the individual description of every slurry milling and castining process. The total mass of the components are found in table 3.2 chapter 3.3.

All slurries were put under vacuum with a magnet stirrer for approximately 1-2 hour before casting.

The casting was first done with a doctor blade, but slurry 14 to slurry 21 was casted on a new tape caster which used a coating bar instead of a doctor blade. The casting on the new tape caster was done with Cu-foil on a plastic foil. The drying temperature on the old caster was 83°C, but on the new 60°C was used.

Slurry 1

Slurry 1 was premixed with a magnet stirrer. First NMP and PVDF were mixed until there were no visible white PVDF particles. Then carbon nanocones were added. The mixing took a couple of hours with magnet the stirrer.

The premixed slurry was milled for 20 minutes at 150 rpm. It had too low viscosity.

Total ball milling time: 20 minutes.

It was then tape casted with a doctor blade on plastic. This didnot work properly as the slurry was too little viscous . It retracted on the plastic.

Slurry 2

Slurry 2 was not premixed. All components were put directly in the milling jar.

The slurry was ball milled for 20 minutes at 150 rpm. It had too low viscosity.

Total ball milling time: 20 minutes.

It was not tape casted.

Slurry 3

Slurry 3 was not premixed. All components were put directly in the milling jar.

The slurry was ball milled for 20 minutes at 150 rpm. It had too low viscosity.

Total ball milling time: 20 minutes.

It was not tape casted. Tested drops for wetting properties on plastic and copper foil. It wetted Cu-foil good, but not the plastic.

Slurry 4

Slurry 4 was not premixed. All components were put directly in the milling jar.

First the powders and 24,99 g NMP were added and ball milled for 20 minutes at 150 rpm. It was too viscous. Added 4,97 g NMP and ball milled for 20 minutes at 150 rpm. It had too low viscosity, just like slurry 3.

Total ball milling time: 40 minutes.

It was tape casted with a doctor blade on Cu-foil on a plastic foil. It retracted from plastic up to the Cu-foil and cracked during drying.

Slurry 5

Slurry 5 was not premixed. All components were put directly in the milling jar.

First the powders and 27,51 g NMP were added and ball milled for 20 minutes at 150 rpm. It looked like slurry 4 with 24,99 g NMP, thereofre 1.06 g NMP was added and the slurry was milled for 20 minutes at 150 rpm. It looked usable, but there was too little for casting at this viscosity. Another 1,00 g NMP was added and the slurry was milled for 20 minutes at 150 rpm. This time it looked good.

Total ball milling time: 1 h.

It was doctor blade casted on Cu-foil on a plastic foil. The slurry looked like it was flowing slowly out of the slit and not casting. A couple of bubbles appeared, but the film looked usable.

Slurry 6

Slurry 6 was not premixed. All components were put directly in the milling jar.

First the powders and 57,03 g NMP was added and milled for 20 minutes at 150 rpm. It was very viscous, like toothpaste. 0,98 g NMP was added and the slurry was milled for 20 minutes at 150 rpm. Still too viscous, but a little more runny. Another 0,49 g NMP was added and the slurry was milled for 20 minutes at 150 rpm. It was too viscous, therefore 0,50 g NMP was added and the slurry was milled for 20 minutes at 150 rpm. The slurry was still too viscous, and another 1,01 g NMP was added and the slurry was milled for 20 minutes at 150 rpm. This time it looked better.

Total ball milling time: 1 hours 40 minutes.

It was tape casted with a doctor blade on plastic. It looks good, seems like a good viscosity. The finished film was flexible and tough.

Slurry 7

Milling time experiment.

Slurry 7 was not premixed. All components were put directly in the milling jar.

The slurry was milled for 5x20 minutes, where it went from high viscosity to lower viscosity after 40 minutes of milling; between 20 and 40 minutes. Then milling was done for 2 more hours, and still had the low viscosity. 16 hours 30 minutes more at 150 rpm gave same result. It did not change after standing still for 45 hours either.

Total ball milling time: 19 hours 50 minutes

It was not tape casted.

Slurry 8

This slurry was made in search of the point of viscosity change.

Slurry 8 was not premixed. All components were put directly in the milling jar.

The slurry was first milled for 20 minutes at 150 rpm. It was too viscous. Then it was milled for 20x1 minutes, checking every minute. It did not change much, but it looked like the viscosity had decreased to some degree. The slurry was still too viscous. Then it was milled for another 20 minutes at 150 rpm and reached the point of viscosity change.

Total ball milling time: 1 h.

It was tape casted with a doctor blade on plastic. Retraction of the slurry was observed.

Slurry 9

This slurry was made in search of the point of viscosity change.

Slurry 9 was not premixed. All components were put directly in the milling jar.

The slurry was first milled for 40 minutes at 150 rpm, then 5 minutes intervals at 150 rpm until it reached the point of viscosity change. After the 9th time it was still too viscous. After the 10th time the viscosity changed. To be sure 2x5 minutes extra milling was done.

Total ball milling time: 1 hours 40 minutes.

It was tape casted with a doctor blade on plastic and did not retract much. Still, it did not seem like it was a good tape casting, as it looked like the slurry ran out of the slit of the doctor blade.

Slurry 10

This slurry was made in search of the point of viscosity change.

Slurry 10 was not premixed. All components were put directly in the milling jar.

The slurry was first milled for 90 minutes at 150 rpm. Then 5 minutes intervals at 150 rpm was done. The 8th interval gave a less viscous slurry. After that the slurry was milled for 2x5 minutes at 150 rpm. Then the slurry was put on a 15 hours and 30 minutes long period of milling to see if it got more viscous as the particles might get smaller of the milling. This was not the case, as it still had the low viscosity.

Total ball milling time: 17 hours 50 minutes.

It was not tape casted.

Slurry 11

Slurry 11 was premixed. The PVDF and NMP was mixed in a magnet stirrer before it was added into the ball milling jar together with the carbon cone powder.

The slurry was milled for 3x20 minutes at 150 rpm. It reached the point of viscosity change after the third round.

Total ball milling time: 1 h.

It was not tape casted.

Slurry 12

Slurry 12 was not premixed. All components were put directly in the milling jar.

The slurry was first milled for 2 hours at 150 rpm. It was too viscous. Then the slurry was milled for 4x1 hours at 150 rpm. It did not change much. After that the slurry was milled for 12 hours at 150 rpm and reached the point of viscosity change.

Total ball milling time: 18 h.

It was not tape casted.

Slurry 13

Slurry 13 was premixed. The PVDF and NMP was mixed in a magnet stirrer before it was added into the ball milling jar together with the carbon cone powder.

The slurry was first milled for 2 hours at 150 rpm. It was too viscous. Then it was milled for 2 hours and 3 hours at 150 rpm. After both times it was still too viscous. Then there was a pause for 14 hours before milling for 3x2h at 150 rpm. It became less viscous, but still too viscous. There were another pause of 19h 25 minutes before another round of 3x2h of ball milling at 150 rpm. The slurry looked like it was closing in on a useful viscosity. Then another pause of 16h 20 minutes was taken before ball milling for 2 hours at 150 rpm. This did not change the slurry viscosity.

Total ball milling time: 21 h.

It was not tape casted.

Slurry 14

New tape casted with bars were used.

Slurry 14 was not premixed. All components were put directly in the milling jar.

First the powders and 25,00 g NMP was put in the milling jar and milled for 16 hours at 150 rpm. It was a bit too viscous for the new type of tape caster. Another round of ball milling of 10 minutes at 150 rpm to see if it got better. It did not. The 1,00 g NMP was added and the slurry was milled for 20 minutes at 150 rpm. This was not good enough. Added 0,98 g NMP and milled for 20 minutes. Looked good.

Total ball milling time: 16 hours 50 minutes.

It was tape casted with with thickest coating bar, 100 μm. It cast looked good.

Slurry 15

Slurry 15 was not premixed. All components were put directly in the milling jar.

The slurry was first milled for 2h 40 minutes at 150 rpm, but it was too viscous. It did not reach the point of viscosity change. Then it was milled for 5x20 minutes at 150 rpm, but again it was too viscous. Overnight milling for 15 hours at 150 rpm made it reach the point of viscosity change. Another 5 minutes of milling at 150 rpm was done to mix the slurry beacuse it had been standing still.

Tota ball milling time: 19 hours 25 minutes.

It was tape casted with thickest coating bar, 100 μm. Some contraction was observed on the plastic.

Slurry 16

Slurry 16 was not premixed. All components were put directly in the milling jar.

The slurry was first milled for 1h 40 minutes at 150 rpm. This was not enough. The slurry was then milled for another 20 minutes at 150 rpm, and then for 1 hour at 150 rpm. This was not enough. Another 5 minutes of milling at 150 rpm was done. The balls made sounds similar to the sounds they made when the slurry had reached the point of viscosity change. The balls might be sticking to the walls beacuse of the viscous slurry. The slurry was then milled for another 5 minutes at 250 rpm which gave sound from the milling balls indicating that they were milling. This milling was not long enough. Another 20 minutes of milling at 250 rpm was done and the slurry reached the point of viscosity change.

Total ball milling time: 3 hours 5 minutes at 150 rpm, and 25 minutes at 250 rpm.

It was tape casted with thickest coating bar, 100 μm. The cast retracted from plastic before it dried.

Slurry 17

Slurry 17 was not premixed. All components were put directly in the milling jar.

The slurry was first put on a milling program overnight, but did not start. The components were in the container the whole night. It was milled for 3x5 minutes at 250 rpm in the morning. It was enough for it to get less viscous.

Total ball milling time: 15 minutes at 250 rpm.

It was bar casted with second thickest bar, 80 μm. The cast looked good.

Slurry 18

Slurry 18 was not premixed. All components were put directly in the milling jar.

The slurry was first milled for 14 hours at 150 rpm. It was too viscous. Then it was milled for another 30 minutes at 150 rpm, and it still looked a little bit too viscous. It had not reached the point of viscosity change. Another 20 minutes of milling at 150 rpm, and it had reached the point of viscosity change.

Total ball milling time: 14 hours 50 minutes.

It was tape casted with second and third thickest coating bar, 80 and 60 μm respectively. The casts looked good, but the third thinnest showed an uneven surface.

Slurry 19

Slurry 19 was not premixed. All components were put directly in the milling jar.

The slurry was milled for 12 hours at 150 rpm. It looked good, but got milled for 5 minutes at 150 rpm to be sure it is properly mixed.

Total ball milling time: 12 hours 5 minutes.

It was tape casted with third thickest coating bar, 60 μm.

Slurry 20

Slurry 20 was not premixed. All components were put directly in the milling jar.

The slurry was milled for 17 hours at 150 rpm. It was too viscous. The slurry was milled for another 2 hours at 150 rpm. It was still too viscous. Another milling for 30 minutes at 150 rpm was dont, but the slurry was still too viscous. Milling for 20 minutes at 250 rpm was tried. The slurry looked better, but did not reach the point of viscosity change. Another 20 minutes of milling at 250 rpm made it less viscous. 5 minutes extra milling at 250 rpm was done to be sure that the point of viscosity change was reached.

Total ball milling time: 19 hours 30 minutes at 150 rpm and 25 minutes at 250 rpm.

It was tape casted with second and third thickest coating bar, 80 and 60 μm respectively. The first cast (80 μm) had some signs of bubbles. The second cast was good.

Slurry 21

Slurry 21 was not premixed. All components were put directly in the milling jar.

First the powders and 22.50 g NMP was put in the milling jar and milled for 2 hours at 150 rpm. The slurry was too viscous, so it was milled for 30 minutes at 250 rpm. The slurry was still too viscous and 2.50 g NMP was added and it was milled for 30 minutes at 250 rpm. The slurry was still too viscous. Another 5.00 g NMP was added and then the slurry was milled for 30 minutes at 250 rpm. After this milling it got a good viscosity for tape casting with the coating bar.

Total ball milling time: 2 hours at 150 rpm, 1 hours 30 minutes at 250 rpm.

It was tape casted with the thickest cpating bar, 100 μm. The cast looked good and even.

Appendix B

Complete test result figures

B.1 Charge/discharge

In chapter 4.5 the results of the charge/discharge are presented with only the first charge, first discharge, and the second charge. This is adequate to present the results of irreversible capacity loss and first charge capacity. The figures presented here are the complete test cycles of all the batteries.

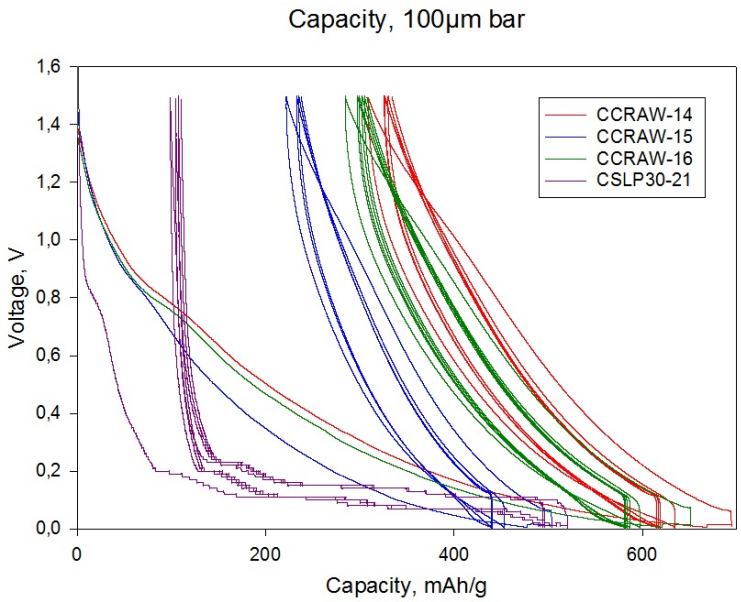

Figure B.1: Charge/discharge cycles for the batteries made with the 100 μm bar.

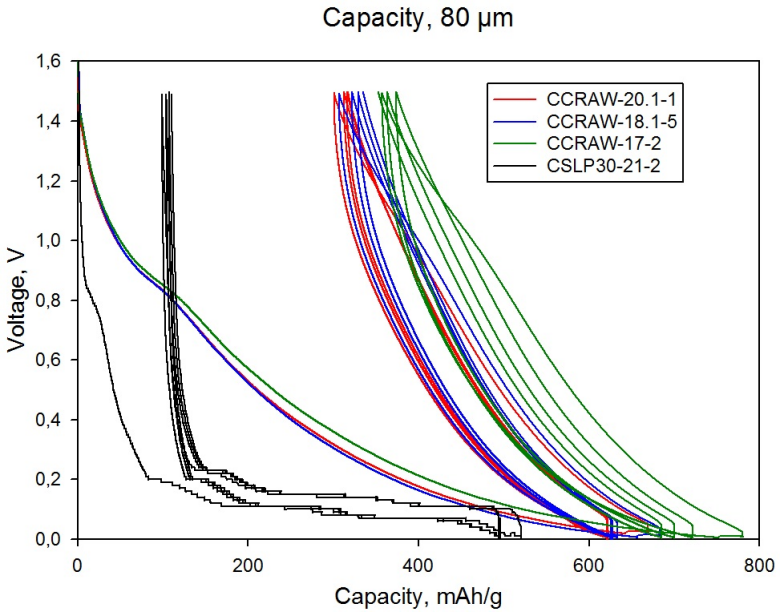

Figure B.2: Charge/discharge cycles for the batteries made with the 80 μm bar.

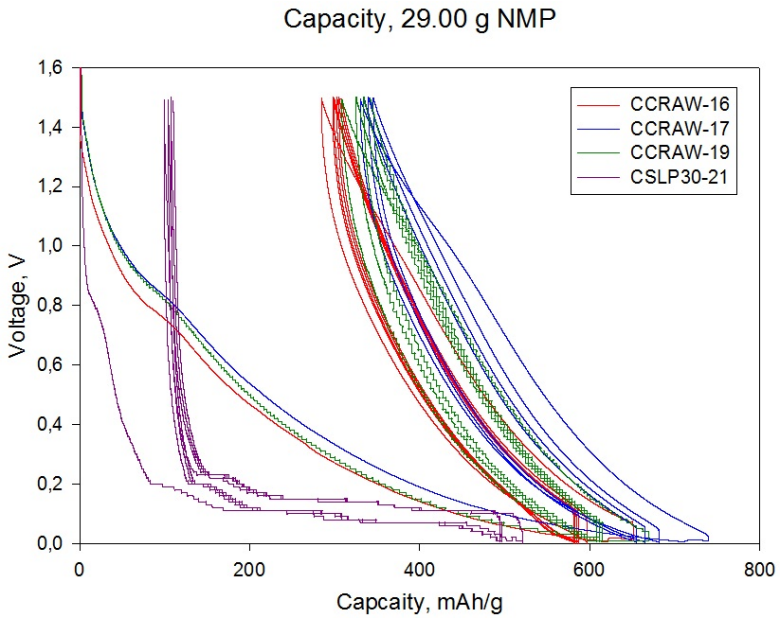

Figure B.3: Charge/discharge cycles for the batteries made of with 29.00 g of NMP.

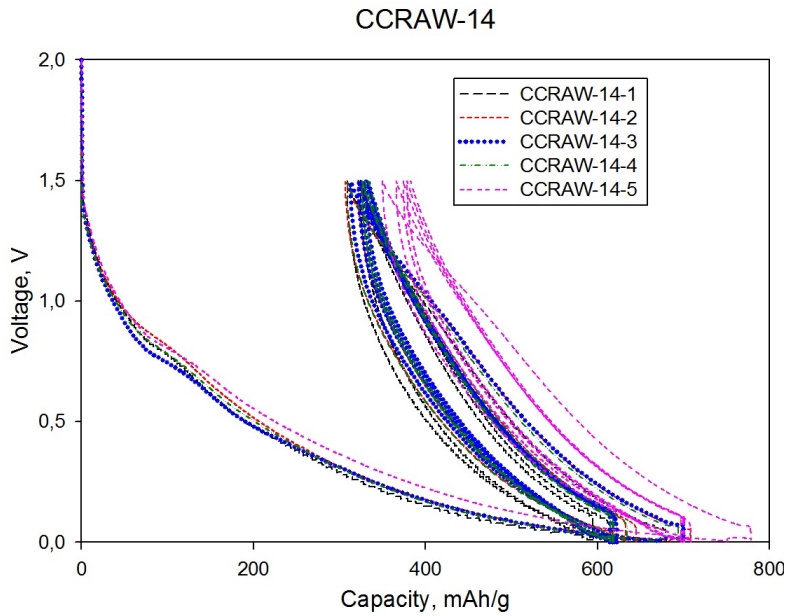

Figure B.4: Charge/discharge cycles for the batteries made of slurry 14.

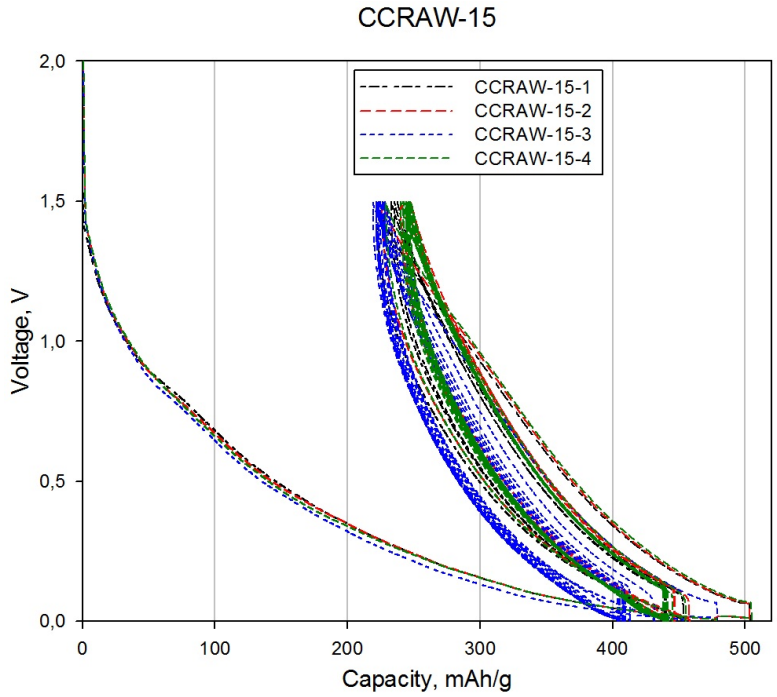

Figure B.5: Charge/discharge cycles for the batteries made of slurry 15.

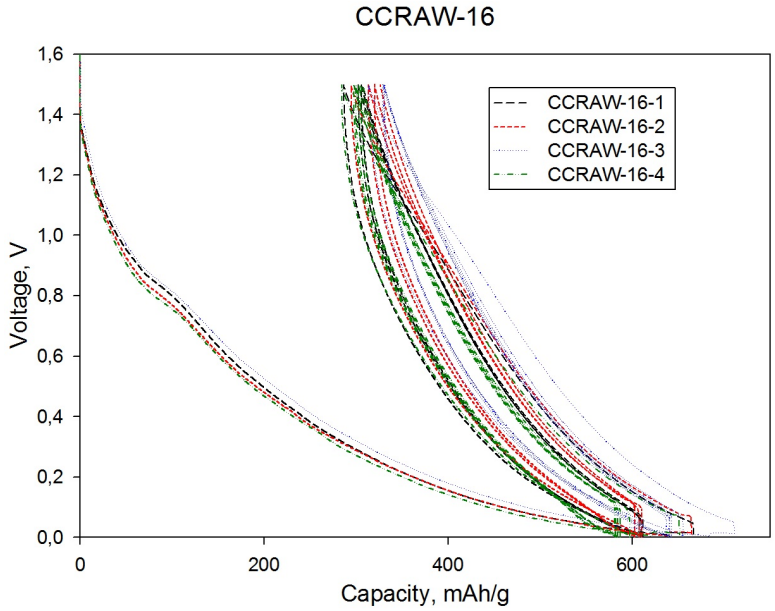

Figure B.6: Charge/discharge cycles for the batteries made of slurry 16.

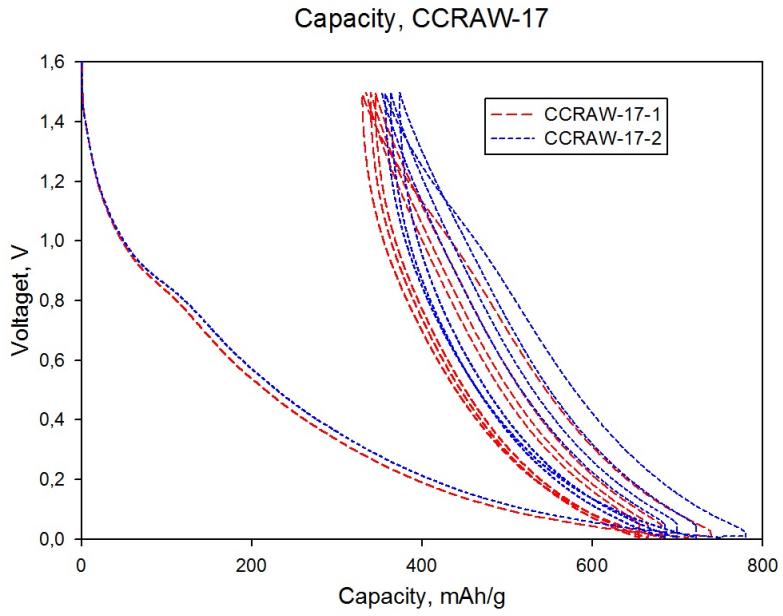

Figure B.7: Charge/discharge cycles for the batteries made of slurry 17.

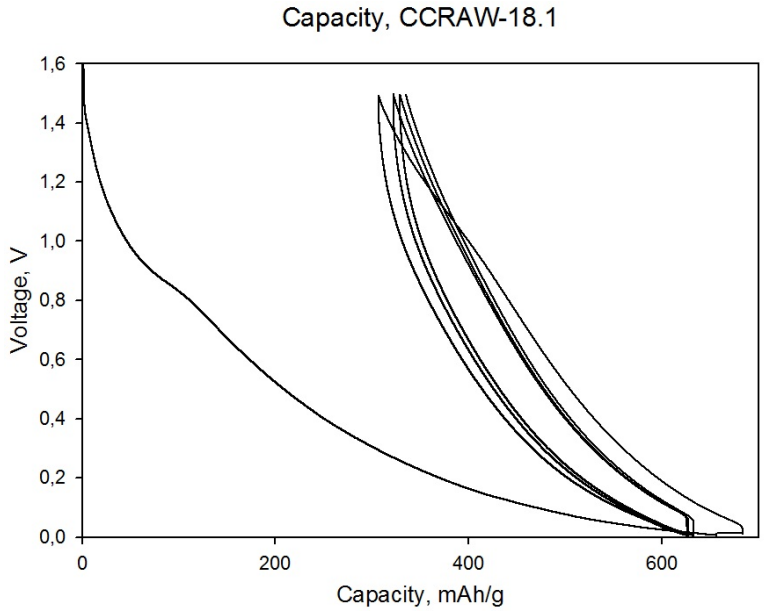

Figure B.8: Charge/discharge cycles for the batteries made of slurry 18, the first cast with the 80 μm bar. .

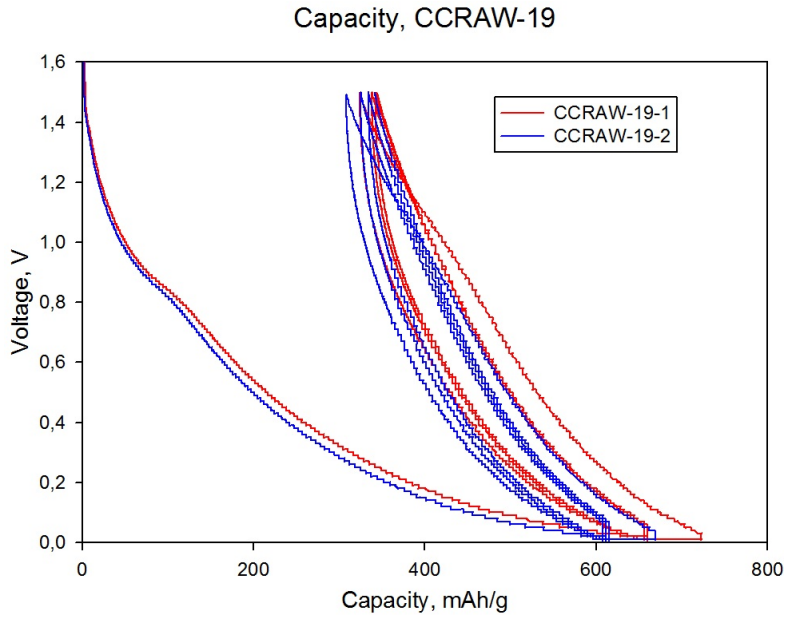

Figure B.9: Charge/discharge cycles for the batteries made of slurry 19.

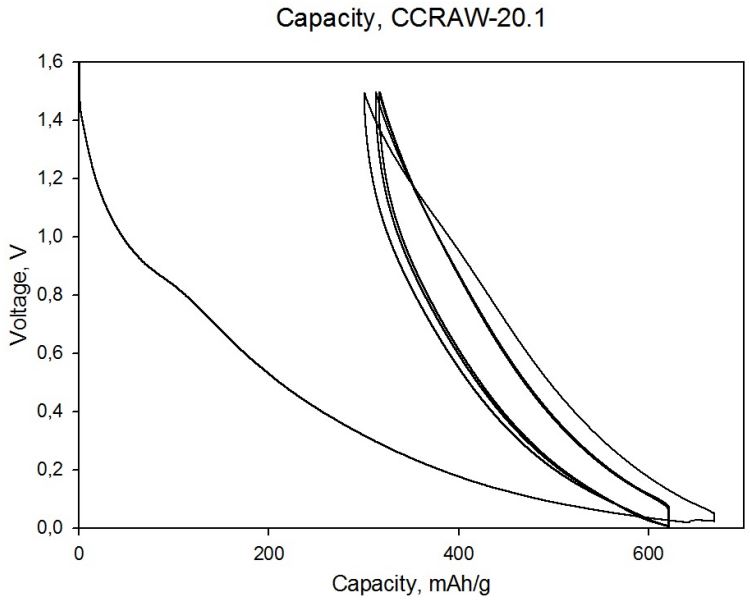

Figure B.10: Charge/discharge cycles for the batteries made of slurry 20, the first cast with the 80 μm bar.

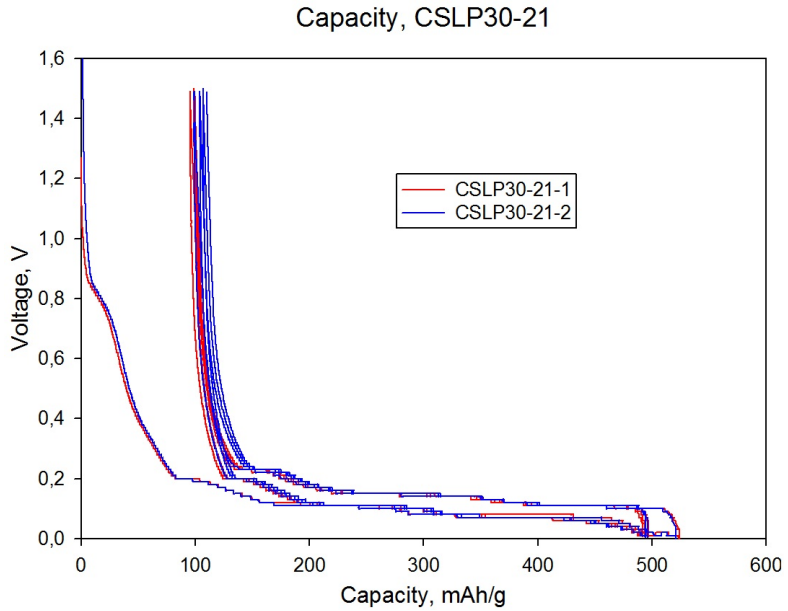

Figure B.11: Charge/discharge cycles for the batteries made of slurry 21.